

Constraining the budget of atmospheric carbonyl sulfide using a 3-D chemical transport model

Michael P. Cartwright^{1,2}, Richard J. Pope^{3,4}, Jeremy J. Harrison^{1,2}, Martyn P. Chipperfield^{3,4}, Chris Wilson^{3,4}, Wuhu Feng^{3,5}, David P. Moore^{1,2} and Parvatha Suntharalingam⁶

5 ¹ School of Physics and Astronomy, Space Park Leicester, University of Leicester, Leicester, UK

² National Centre for Earth Observation, Space Park Leicester, University of Leicester, Leicester, UK

³ School of Earth and Environment, University of Leeds, Leeds, UK

⁴ National Centre for Earth Observation, University of Leeds, Leeds, UK

⁵ National Centre for Atmospheric Science, University of Leeds, Leeds, UK

10 ⁶ School of Environmental Sciences, University of East Anglia, Norwich, UK

Correspondence to: Michael P. Cartwright (mpc24@leicester.ac.uk)

Abstract.

Carbonyl sulfide (OCS) has emerged as a valuable proxy for photosynthetic uptake of carbon dioxide (CO₂) and is known to be important in the formation of aerosols in the stratosphere. However, uncertainties in the global OCS budget remain large, due mainly to three flux terms: vegetation and soil uptake, and oceanic emissions. Bottom-up estimates do not yield a closed budget, thought to be due to unaccounted-for tropical emissions of OCS. Here we present a simulation of atmospheric OCS over the period 2004-2018 using the TOMCAT 3-D chemical transport model aimed at better constraining some terms in the OCS budget. Vegetative uptake of OCS is estimated by scaling gross primary productivity (GPP) output from the Joint UK Land Environment Simulator (JULES), using the leaf relative uptake (LRU) approach. The remaining surface budget terms are taken from available literature flux inventories, and adequately scaled to bring the budget into balance.

The model is compared with limb-sounding satellite observations made by the Atmospheric Chemistry Experiment – Fourier Transform Spectrometer (ACE-FTS) and surface flask measurements from 14 National Oceanic and Atmospheric Administration – Earth System Research Laboratory (NOAA-ESRL) sites worldwide.

We find that calculating vegetative uptake using the LRU underestimates the surface seasonal cycle amplitude (SCA) in the NH mid and high latitudes, by approximately 37 ppt (35%). The inclusion of a large tropical source is able to balance the global budget, but further improvement to the SCA and phasing would likely require a flux inversion scheme.

Compared to co-located ACE-FTS OCS profiles between 5 km and 30 km, TOMCAT remains within 25 ppt (approximately 5% of mean tropospheric concentration) of the measurements throughout the majority of this region and lies within the standard deviation of these measurements. This provides confidence in the representation of atmospheric loss and surface fluxes of OCS in the model. Atmospheric sinks account for 154 Gg S of the annual budget, which is 10 – 50% larger than previous studies. Comparing the surface monthly anomalies from the NOAA-ESRL flask data to the model simulations shows a root mean square error range of 3.3 – 25.8 ppt. We estimate the total biosphere uptake to be 951 Gg S which is in the range of recent inversion studies (893 – 1053 Gg S), but our terrestrial vegetation flux accounts for 629 Gg S of the annual budget, which is

lower other recent studies (657 – 756 Gg S). However, to close the budget, we compensate this with a large annual oceanic emission term of 689 Gg S, focused over the tropics, which is much larger than bottom-up estimates (285 Gg S). Hence, we agree with recent findings that missing OCS sources likely originate from the tropical region.

This work shows that satellite OCS profiles offer a good constraint on atmospheric sinks of OCS through the troposphere and stratosphere and are therefore useful for helping to improve surface budget terms. This work also shows that the LRU approach is an adequate representation of the OCS vegetative uptake, but this method could be improved by various means, such as using a higher resolution GPP product or plant-functional-type-dependent LRU. Future work will utilise TOMCAT in a formal inversion scheme to better quantify the OCS budget.

1 Introduction

Carbonyl sulfide (OCS) is the most abundant of all sulfur-containing gases in the atmosphere and is important due to its potential use as a proxy for the photosynthetic uptake of carbon dioxide (CO₂) by vegetation (Sandoval-Soto et al., 2005; Montzka et al., 2007; Campbell et al., 2008; Suntharalingam et al., 2008; Blonquist et al., 2011; Berry et al., 2013; Launois et al., 2015b). Furthermore, due to its oxidation in the stratosphere, OCS is the largest source of sulfuric acid in the stratospheric aerosol layer in times of low volcanic activity (Crutzen, 1976; Kremser et al., 2016). In the troposphere, OCS has a global mean mixing ratio (mole fraction) of approximately 480 parts per trillion (ppt) and a lifetime of approximately 2.5 years (Montzka et al., 2007). In the stratosphere the OCS mixing ratio declines strongly with increasing altitude, due to photochemical removal and the only source being transport from the troposphere. The stratospheric lifetime is approximately 64 ± 21 years (Barkley et al., 2008), ranging from 54.1 ± 9.7 years in the sub-tropics to 103.4 ± 18.3 years in the Antarctic (Hannigan et al., 2022). The long stratospheric partial lifetime (defined as total atmospheric OCS burden divided by loss in stratosphere) reflects the low total mass of OCS there, giving a smaller absolute loss, and the low OH concentration compared to the troposphere.

Observations of OCS by the Network for the Detection of Atmospheric Composition Change (NDACC) using ground-based solar-viewing Fourier Transform Infrared Spectrometers (FTIR) show weak positive trends between 2009 and 2016 in the troposphere at most of the 22 measurement sites of <1% yr⁻¹ (Hannigan et al., 2022). Stronger positive trends, up to 1.93±0.26% yr⁻¹ for 2009-2016, are observed in the stratosphere above all sites, except tropical sites, Mauna Loa and Altimoni, which show a negative trend (approximately -0.5% yr⁻¹). Furthermore, a downturn in free tropospheric OCS concentration reveals a negative trend between 2016 and 2020 at all sites (Hannigan et al., 2022). Kremser et al. (2015) showed positive OCS trends between 2001 and 2015, determined from ground-based FTIR total column measurements at 3 southern hemisphere (SH) sites (also used by Hannigan et al., 2022) and driven by changes in the tropospheric column. In contrast, the National Oceanic and Atmospheric Administration - Earth System Research Laboratory (NOAA-ESRL) global monitoring network has 14 sites and shows no consistent trend in surface OCS at any one location during the period of 2000 to 2005 (Montzka et al., 2007). Additionally, Glatthor et al. (2017) concluded that the tropospheric OCS budget is balanced based on a global Michelson

Interferometer for Passive Atmospheric Sounding (MIPAS) satellite dataset (2002-2012), whilst ground-based partial-column measurements at the Jungfraujoch (46.5°N, 8.0°E) showed no significant trend in the free troposphere between 2008 and 2015 (Lejeune et al., 2017).

70 One of the main sources of atmospheric OCS is oceanic emission, with total estimates ranging from 230 to 992 Gg S yr⁻¹ (Kettle et al., 2002; Montzka et al., 2007; Suntharalingam et al., 2008; Berry et al., 2013; Glatthor et al., 2015; Kuai et al., 2015; Launois et al., 2015a; Lennartz et al., 2021; Ma et al., 2021; Remaud et al., 2022). Oceanic emission has 3 main contributions: direct emission of OCS, oxidation of emitted dimethyl sulphide (DMS) and oxidation of emitted carbon disulphide (CS₂). Both light-dependent (photochemical) and light-independent production play a role in oceanic emission (Launois et al., 2015a), the former linked primarily to incident UV radiation at the sea surface and the latter far below the surface. Both are driven by biological production and are proportional to amounts of chromophoric dissolved organic matter (CDOM), especially at the surface, where it can act to absorb some of the available light (Lennartz et al., 2021). Furthermore, Lennartz et al. (2021) suggest the importance of direct ocean-emitted OCS and oxidized CS₂ exceeds that of oxidized DMS which accounts for only a small portion of the overall ocean borne OCS emissions.

80 Vegetative uptake is the most important sink of atmospheric OCS, and its magnitude is significantly more uncertain than the ocean flux, with estimates ranging from 210 to 2400 Gg S yr⁻¹ (Kettle et al., 2002; Sandoval-Soto et al., 2005; Suntharalingam et al., 2008; Berry et al., 2013; Glatthor et al., 2015; Kuai et al., 2015; Launois et al., 2015b; Kooijmans et al., 2021; Ma et al., 2021; Maignan et al., 2021; Remaud et al., 2022). OCS is consumed during the photosynthesis process, which proceeds along the same enzymatic pathways as CO₂ (Protoschill-Krebs et al., 1996). However, unlike for CO₂, this process is one-way due to the irreversible OCS hydrolysis reaction, catalysed by carbonic anhydrase (Protoschill-Krebs et al., 1996). OCS hydrolysis 85 also occurs in soil, primarily catalysed by carbonic anhydrase contained in bacteria and fungi (Kesselmeier et al., 1999; Smith et al., 1999; Li et al., 2005; Seibt et al., 2006; Kato et al., 2008), as well as by other enzymes, such as nitrogenase, CO dehydrogenase and CS₂ hydrolase (Smith and Ferry, 2000; Masaki et al., 2021). Soil uptake is the second largest OCS sink, with an estimated annual net loss of 30 – 355 Gg S (Kettle et al., 2002; Montzka et al., 2007; Berry et al., 2013; Glatthor et al., 2015; Kuai et al., 2015; Kooijmans et al., 2021; Abadie et al., 2022). Other findings suggest that the seasonal variation in OCS 90 soil uptake is relatively weak in boreal forest regions, but shows dependency on soil moisture (Sun et al., 2018). Soil has also been observed to act as an emitter of OCS in certain conditions, dependent on such components as temperature, soil moisture, nitrogen content and incident solar radiation (Whelan et al., 2013; Maseyk et al., 2014; Spielmann et al., 2019; Kitz et al., 2020).

95 Chin and Davis (1993) presented one of the first attempts at quantifying the global OCS (and CS₂) budget terms, but these were subject to substantial uncertainties. However, multiple terms, such as atmospheric loss and volcanism, were subsequently used in the estimates presented by Watts (2000) and Kettle et al. (2002), the latter of which has been used as a benchmark for more recent studies (Montzka et al., 2007; Suntharalingam et al., 2008; Berry et al., 2013; Glatthor et al., 2015; Kuai et al., 2015). Analysis of flask and aircraft data spanning both hemispheres by Montzka et al. (2007) have offered the most significant updates since the aforementioned studies and suggest a vegetative sink (1115 Gg S yr⁻¹) up to five times larger than the estimate

100 (240 Gg S yr⁻¹) presented by Kettle et al. (2002). Due to the negligible or weak-positive atmospheric OCS trend up to 2016, this would suggest a larger source is required for balance. The general consensus is that this must originate in the tropical oceans, due to measurement peaks from satellite and aircraft observations (Glatthor et al., 2015; Kuai et al., 2015), as well as modelling estimates pointing to this region as an underestimated source (Berry et al., 2013; Launois et al., 2015a; Remaud et al., 2022). There is opposition from Lennartz et al. (2017, 2021), who estimate global oceanic emissions to be approximately
105 285-345 Gg S yr⁻¹, derived using a global oceanic box model and measurements of surface waters, thus too low to account for this difference entirely. A recent study has also suggested there is an underestimation in previous gridded anthropogenic OCS flux inventories by 200 Gg S yr⁻¹, which could account for some of the deficit (Zumkehr et al., 2018), supported by measurements of OCS in firm air and ice core samples (Aydin et al., 2020). Top-down estimates by Ma et al. (2021), using an inversion scheme that assimilates surface flask observations, point to a tropical source of unknown origin but the inversion
110 setup presented by Remaud et al. (2022) suggests a large tropical OCS source of oceanic origin. Both studies downplay the likelihood if it being of exclusively oceanic origin, hence there is still substantial uncertainty in several of the global surface fluxes of OCS. These recent studies quantifying OCS flux inventories show less uncertainty than previous ones. However, to improve the inventories further, increased spatial coverage by ground-based and remote atmospheric OCS observations are required, as well as OCS flux measurements (Whelan et al., 2018).

115 In this study, we add a further model (TOMCAT) to those already employed to simulate global OCS distribution, with emphasis on a full vertical comparison extending through the troposphere and stratosphere (approximately 5 – 35 km). Three inventories of fluxes are used to drive the model in separate experiments, offering different perspectives. Firstly, a control setup using fluxes from Kettle et al. (2002), the results of which are denoted TOMCAT_{CON}. Secondly, we constructed an inventory using modified fluxes from Kettle et al. (2002) in addition to a vegetative uptake flux quantified using Gross Primary Productivity
120 (GPP) in the leaf relative uptake (LRU) approach (Campbell et al., 2008; Stimler et al., 2012; Asaf et al., 2013) and one flux from the literature, i.e. anthropogenic emissions from Zumkehr et al. (2018). The model simulation using this array of fluxes is referred to as TOMCAT_{OCS}. Finally, we compiled an inventory using newly available bottom-up fluxes from recent literature, TOMCAT_{SOTA} (TOMCAT_{State-Of-The-Art}). Each inventory of OCS fluxes is used in the TOMCAT 3-D chemical transport model (CTM) over the time period 2004 – 2018, providing fresh insight into the magnitude and location of the fluxes
125 of OCS and how this translates vertical information of OCS into improved understanding of both surface and atmospheric fluxes. Furthermore, to investigate differences in Southern Hemisphere (SH) stratospheric mixing ratios between TOMCAT_{OCS} and satellite observations, additional simulations were performed to assess the influence of a hypothetical reduction in stratospheric photolysis would have on OCS distribution.

Section 2 summarises the data used for evaluating the model. The model setup and each flux inventory are described in Sect.
130 3. Results and comparisons with tropospheric and stratospheric satellite observations from the Atmospheric Chemistry Experiment infrared Fourier transform spectrometer instrument (Bernath, 2017; Boone et al., 2020) and measurements made by the NOAA-ESRL flask network (Montzka et al., 2007) are shown in Sect. 4, discussed further in Sect. 5 and concluding remarks are presented in Sect. 6.

2 Observations

135 2.1 Atmospheric Chemistry Experiment – Fourier Transform Spectrometer Observations

Onboard SCISAT (Science Satellite), launched in August 2003, is the Atmospheric Chemistry Experiment infrared Fourier transform spectrometer (ACE-FTS), which operates in a solar occultation mode measuring radiation between 750 and 4400 cm^{-1} at a spectral resolution of 0.02 cm^{-1} (Bernath et al., 2005; Bernath, 2017). Although the planned SCISAT mission duration was only two years, it now has a data record spanning 19 years. This longevity makes the ACE-FTS a valuable tool for
140 measuring atmospheric trace gases and characterising their variability and trends. Atmospheric trace gas profiles are retrieved using a non-linear least squares global-fit approach on the measurement altitude grid (3 km vertical resolution), then interpolated on to a uniform 1 km grid. ACE-FTS is capable of measuring profiles for a number of trace gases, including OCS, from 5 km (or cloud top) up to about 30 km. OCS is retrieved using microwindows of various widths between 2039.01 and 2057.52 cm^{-1} , including a band at 1950.10 cm^{-1} to minimise the impact of H_2O interference. Because the primary science
145 mission of ACE-FTS is to measure atmospheric ozone distributions over Canada, the satellite's orbit is such that approximately 60% of all measurements are at latitudes poleward of $\pm 60^\circ$. However, over the course of a year measurements are taken over a wide range of latitudes, providing a wealth of data with which to validate global CTM simulations. For this study, ACE-FTS version 4.1 (hereafter ACE) retrieved profiles from February 2004 to December 2018 (approximately 98,000 profiles) (Boone et al., 2020) were used in the validation of the modelled TOMCAT OCS distribution. The version 4.1 retrievals incorporate a
150 new instrumental line shape (Boone and Bernath, 2019) and utilise the 2016 High-Resolution TRANsmission molecular absorption database (HITRAN) data (Gordon et al., 2017). Systematic errors in OCS measurements occur as a result of contamination from other gases in the microwindow (and clouds), while random errors are induced by random fitting errors from the least squares analysis, both have generally been improved in the version 4.1 product, over version 3.6 (Boone et al., 2020). The errors in ACE OCS measurements amount to a mean of approximately 3.8% throughout the entire profile globally.
155 In the lower troposphere, below 10 km, errors are larger, approximately 7.2% and above 20 km, are relatively low, at 3.4%.

2.2 NOAA-ESRL Flask Measurements

The surface OCS measurements described here are shown in Sect. 4; here we present a summary of the method of data collection (performed by the NOAA-ESRL network) and the site information (see Table 1). Flasks of ambient air have been collected approximately 1 to 5 times per month at 14 measurement sites across both hemispheres since early 2000.
160 Measurements of the OCS concentrations within the flasks are made using gas chromatography and mass spectrometry at the NOAA-ESRL Boulder laboratories (Montzka et al., 2007). In this study, we use data from all the Halocarbons & other Atmospheric Trace Species (HATS) surface measurement sites for the purpose of validating the surface OCS concentrations from the TOMCAT model.

Table 1. NOAA-ESRL flask sampling site information for OCS measurements (Montzka et al., 2007).

Code	Name	Country	Latitude (°N)	Longitude (°E)	Elevation (metres)
ALT	Alert, Nunavut	Canada	82.5	-62.5	185
BRW	Utqiagvik (formerly Barrow), Alaska	United States	71.3	-156.6	11
CGO	Kennaook / Cape Grim, Tasmania	Australia	-40.7	144.7	94
HFM	Harvard Forest, Massachusetts	United States	42.5	-72.2	340
KUM	Cape Kumukahi, Hawaii	United States	19.6	-155.0	8
LEF	Park Falls, Wisconsin	United States	45.9	-90.3	472
MHD	Mace Head, County Galway	Ireland	53.3	-9.9	5
MLO	Mauna Loa, Hawaii	United States	19.5	-155.6	3397
NWR	Niwot Ridge, Colorado	United States	40.1	-105.6	3523
PSA	Palmer Station	Antarctica (United States)	-64.8	-64.1	10
SMO	Tutuila	American Samoa	-14.2	-170.6	42
SPO	South Pole	Antarctica (United States)	-90.0	-24.8	2810
SUM	Summit	Greenland	72.6	-38.4	3210
THD	Trinidad Head, California	United States	41.1	-124.2	107

3 Chemical transport modelling of OCS

3.1 TOMCAT Model Setup

We have used the TOMCAT 3-D off-line CTM (Chipperfield, 2006; Monks et al., 2017) to model atmospheric OCS. This model has been used in a wide range of studies, including to better constrain methane flux estimations (Wilson et al., 2016;

Parker et al., 2018), as a forward model for methane flux inversions (McNorton et al., 2018) and to investigate stratospheric ozone depletion (Claxton et al., 2019). In this work, TOMCAT is driven by meteorological reanalysis data (ERA-Interim) from the European Centre for Medium-Range Weather Forecasts (ECMWF, Dee et al., 2011). ERA-Interim convective mass fluxes are used following the scheme presented in Feng et al. (2011). The model distribution of OH is specified from pre-computed fields which vary monthly, but not inter-annually. The monthly distributions are taken from Spivakovsky et al. (2000) and scaled by a factor of 0.92 in accordance with Huijnen et al. (2010). The photolysis loss is based on precomputed rates from the full chemistry version of TOMCAT (Monks et al., 2017). Atmospheric OH loss accounts for approximately 120 – 130 Gg S yr⁻¹ (roughly 10% of the total OCS sink) of the TOMCAT_{OCS} budget and photolysis about a quarter of this, 30 – 34 Gg S yr⁻¹ (approximately 3% of the total OCS sink). TOMCAT_{OCS} and TOMCAT_{SOTA} are spun for 10 years prior to 2004, and then run between 2004 and 2018 at a horizontal resolution of approximately 2.8° × 2.8° (T42 Gaussian grid), with 60 atmospheric layers from the surface up to 0.1 hPa, on a time-step of 6 hours. In the case of TOMCAT_{OCS}, the vegetative flux is also calculated every 6 hours. TOMCAT_{CON} is initialised using the distribution of TOMCAT_{OCS} at the end of the spin-up period but is run for just a single year, 2004, due to the negative trend and its purpose in this study as a point of reference, rather than a benchmark for improvement. Surface flux fields of OCS were implemented within TOMCAT on a monthly 1° × 1° grid. Depending on the inventory in use, some vary inter-annually, i.e., vegetative uptake and anthropogenic emission, and the remaining fluxes do not (oceanic emission, soil uptake and biomass burning). These are mapped onto the model grid in a way that conserves local distributions and the total global flux. For comparison with ACE, the geopotential height output from the model is converted to altitude; this is done using the hypsometric equation at a reference pressure of 1000 hPa, and then interpolated on to the 1 km equidistant altitude grid used by ACE-FTS. Furthermore, the profiles outputted by TOMCAT are spatio-temporally co-located with the ACE observations to provide a precise like-for-like comparison. Monthly mean surface concentrations are calculated from the flask observations made by the NOAA-ESRL network and compared with monthly mean TOMCAT output averaged across the time period, used for each respective setup. Co-sampling of the model output with NOAA-ESRL measurements would be a more representative comparison, but here we have not subsampled the model on the specific days of NOAA observations.

195 **3.2 Kettle Flux Inventory**

The fluxes described in this section originate from the literature (Watts, 2000; Kettle et al., 2002; Suntharalingam et al., 2008), and are used to run the control simulation, TOMCAT_{CON}. This model run is utilised as a comparison to the model driven by our new inventory of fluxes described in Sect. 3.3, TOMCAT_{OCS} and to TOMCAT_{SOTA} in Sect. 3.4. TOMCAT_{CON} was initialised using OCS values in each grid box from TOMCAT_{OCS}, after 10 years (1994 – 2003) spin-up and run for only a single year (2004), due to the net negative budget from these fluxes of approximately -46 Gg S yr⁻¹.

Three of the six sources, used to simulate TOMCAT_{CON}, are oceanic: a direct OCS flux term, one due to oxidation of CS₂ and one due to oxidation of DMS. These were converted to OCS emissions using molar conversion factors (Chin and Davis, 1993; Barnes et al., 1994). The OCS and CS₂ emission terms were quantified using a physio-chemical model, the main source being

from photochemical production (Kettle et al., 2002). However, as DMS measurements are more abundant than OCS and CS₂, these were used to parameterize this flux (Kettle and Andreae, 2000). Anthropogenic OCS emissions consist of two factors, a direct term and one from the oxidation of CS₂, the latter being considerably larger. They are both calculated here using SO₂ fields from Watts (2000) due to the extensive datasets available and a relationship between the facilities that release SO₂ and OCS, despite there being no direct chemical reaction (Kettle et al., 2002). The final source term is biomass burning scaled similarly to that in Kettle et al. (2002), but varies according to the monthly climatology of Duncan et al. (2003).

The three sink terms are an oceanic sink, soil uptake and a vegetative sink. The first was quantified using the same physiochemical model used for the OCS and CS₂ source terms described above and covers the periods in the year where the direct oceanic emission of OCS flips from being a source to becoming a sink. These are focused mostly over extra-tropical open ocean regions and during each hemisphere's summer period. Gridded soil uptake was calculated by applying correction factors for temperature, ambient OCS and soil water content to a standardised uptake rate of 10 pmol m⁻² s⁻¹ (Kesselmeier et al., 1999). The monthly mean climatological data for the temperature and soil water content is taken from Sellers et al. (1995), where the soil water content is a percentage of saturation in the top 2 cm of soil. Anoxic soil emissions are neglected in this study but with the availability of new data sets future simulations could include these sources (Abadie et al., 2022; Whelan et al., 2022). Finally, the vegetative uptake is calculated by employing a normalised difference vegetation index (NDVI) to scale net primary productivity (NPP) distribution from Fung et al. (1987). We also scale up this term to the quoted upper limit of 270 Gg S yr⁻¹ by Kettle et al. (2002). As mentioned in Sect. 3.1, removal of atmospheric OCS by OH loss and photolysis is also accounted for in the model.

The spatial distribution for the months of January, April, July and October for the vegetation and soil uptake and oceanic emissions used in TOMCAT_{CON} are presented in the supplement: Fig. S1, S2 and S3, respectively.

3.3 LRU approach and Modified Flux Inventory

TOMCAT_{OCS} uses an array of fluxes that is orientated around a calculated vegetative uptake term, F_{OCS}, using the LRU approach (Campbell et al., 2008; Stimler et al., 2012; Asaf et al., 2013). The calculation of F_{OCS} is explained in Sect. 3.3.1 and a summary of the accompanying fluxes is provided in Sect. 3.3.2, including the full budget in Table 2.

3.3.1 Calculating OCS Vegetative Uptake using Gross Primary Productivity

The new vegetative sink calculation, used in TOMCAT_{OCS}, differs fundamentally from the method described in Sect. 3.2, and used in the control model simulation, as the use of NPP has been shown to underestimate the seasonal amplitude in other modelling studies (Suntharalingam et al., 2008; Berry et al., 2013). Sandoval-Soto et al. (2005) suggested that using NPP to calculate OCS uptake would underestimate the global burden and therefore they recommend using gross primary productivity (GPP) as an alternative. Furthermore, they were the first to quantify deposition velocity ratios for CO₂ and OCS for different plant types, which previous studies had assumed to be equal.

$$235 \quad F_{OCS} = GPP \frac{[OCS]}{[CO_2]} \times LRU, \quad (1)$$

Using Eq. (1) we calculated the vegetative flux of OCS (F_{OCS}), in units of $Gg \text{ S yr}^{-1}$, by scaling GPP ($Gg \text{ C yr}^{-1}$) using a LRU of 1.6; a mean value from gas-exchange measurements of 22 plant species (Stimler et al., 2012). LRU is the ratio of OCS assimilation rates to CO_2 at the leaf-scale, both normalised by their respective mixing ratios, signified by the square brackets in Eq. (1), in units of parts per billion. Fluxes, including F_{OCS} , were implemented in TOMCAT in units of $\text{molecules cm}^{-2} \text{ s}^{-1}$

240 Each time-step in the model a new F_{OCS} value is calculated, as $[OCS]$ is the mixing ratio from the previous time-step, starting at a value of 500 ppt in 1994. The use of a constant LRU value was found to contribute less to error in the calculation of F_{OCS} than differences in GPP between models on a continental scale by Hilton et al. (2017). However, Maignan et al. (2021) found the opposite, that 70% of uncertainty was attributed to the use of three different LRU datasets and 40% when considering three land surface models. As there are available plant-functional-type dependent LRU datasets, implementing spatially varying

245 LRU values will be undertaken in future work (Seibt et al., 2010; Maignan et al., 2021). The GPP flux used in our calculation, generated by the Joint UK Land Environment Simulator (JULES) model, applies the WATER and Global CHange (WATCH) Forcing Data methodology to ERA-Interim reanalysis (WFDEI) between 1979 and 2012 and uses Global Precipitation Climatology Centre (GPCC) precipitation data (Slevin et al., 2016). Monthly mean gridded CO_2 surface mixing ratios, used in the calculation of F_{OCS} , came from a TOMCAT simulation which assimilated surface flask concentrations for 2010 (see Fig.

250 S4 in the supplement) (Gloor et al., 2018). Given that 2010 is situated approximately in the middle of the study period, it should be a reasonable estimate of the long-term average. Therefore, the GPP data used was also for 2010, given its relatively small inter-annual variability (Chen et al., 2017). As we compare only monthly means at the surface and seasonal OCS to ACE, long-term inter-annual variability was not considered in the scope of this work. However, future work using TOMCAT can exploit longer-term records of surface CO_2 mixing ratios and GPP. Our resulting estimate of the mean global yearly value

255 of F_{OCS} between 2004 and 2018 is $629 Gg \text{ S}$, which is nearly three times the value of Kettle et al. (2002) $240 Gg \text{ S}$ and over half that of the largest estimation of $1115 Gg \text{ S}$ by Montzka et al. (2007) in Table 2, and under half that estimated by Launois et al. (2015b), $1335 Gg \text{ S yr}^{-1}$, using the Organising Carbon and Hydrology In Dynamic Ecosystems (ORCHIDEE) land surface model. The spatial distribution of F_{OCS} for the months of January, April, July, and October, in 2010 only, is presented in the supplement: Fig. S5.

260 3.3.2 Scaling of OCS Prior Fluxes to Balance OCS Budget

As the fluxes described in Sect. 3.2 are utilised in constructing the inventory for $TOMCAT_{OCS}$, with the exception of calculating the vegetative uptake and anthropogenic emissions (which are taken from Zumkehr et al., 2018), the fluxes must be modified to suitably close the overall budget, which we assume to be in balance due to a negligible or weak trend in the majority of the study period (Montzka et al., 2007; Kremser et al., 2015; Glatthor et al., 2017; Lejeune et al., 2017; Hannigan et al., 2022). As

265 F_{OCS} is larger than the vegetative uptake term than that of Kettle et al. (2002), we scale up several of the emission terms

described in Sect. 3.2, although some of the difference was accounted for in the larger anthropogenic emissions. Furthermore, some of the fluxes were adjusted to better represent recent estimations in the literature, i.e., soil uptake.

270 TOMCAT_{OCS} makes use of anthropogenic OCS emissions presented by Zumkehr et al. (2018). Like Kettle et al. (2002), anthropogenic OCS emissions consist of two factors, a direct term and one from the oxidation of CS₂, the latter being considerably larger. Eleven anthropogenic sources of OCS were quantified by Zumkehr et al. (2018) for the period 1980 – 2012, the largest contributions originating from residential and industrial coal usage and the rayon industry. Emission factors for each source are applied to country-scale industrial activity data, obtained from a wide range of sources, then gridded spatially and temporally based on a gridded proxy flux (Zumkehr et al., 2018).

275 Scaling OCS emitted from biomass burning (as described in Sect. 3.2) and anthropogenic sources was not considered suitable to balance increases to sink terms, as these are less uncertain than oceanic emissions. Furthermore, biomass burning is more focused in lower latitude agricultural regions and anthropogenic emissions tend to be focused over point sources, mostly in Asia.

The soil flux utilised for TOMCAT_{OCS} was calculated by Kettle et al. (2002) using the method described in Sect. 3.2 and assumes a constant 500 ppt OCS ambient value in the scaling of the standardised uptake. Soil uptake was scaled by 2.5 times
280 from 130 Gg S yr⁻¹ to 322 Gg S yr⁻¹ to bring it in line with literature findings that estimate soil uptake to be between 236 – 507 Gg S yr⁻¹ (Berry et al., 2013; Launois et al., 2015b; Ma et al., 2021; Remaud et al., 2022). These studies used different approaches; Berry et al. (2013) use a global carbon cycle model, SiB 3, to obtain a new estimate of soil uptake based on empirical data and a mechanistic understanding of the processes influencing OCS diffusion into soil. Launois et al. (2015b) use H₂S soil deposition to infer OCS fluxes, as this is a by-product of the OCS hydrolysis reaction and therefore a proxy for
285 OCS uptake. Ma et al. (2021) and Remaud et al. (2022) use inverse frameworks, the former estimate a combined vegetative and soil uptake of 1053 Gg S yr⁻¹ and the latter estimate a soil uptake of 236 Gg S yr⁻¹. Recent work using mechanistic soil uptake models (Ogée et al., 2016) suggest oxic soil uptake is lower than the estimates discussed here: Kooijmans et al. (2021) estimate an annual uptake of 89 Gg S yr⁻¹ and Abadie et al. (2022) estimates 126 Gg S yr⁻¹. These values do not yet align with inversion studies, adding to the uncertainty in surface fluxes, especially in the tropics, that accounts for a large portion of
290 terrestrial OCS uptake (Ma et al., 2021; Remaud et al., 2022).

Initial testing of our new fluxes in TOMCAT yielded low-biased simulated OCS concentrations at Northern Hemisphere (NH) NOAA-ESRL sites, ALT, BRW and MHD, but a seasonal cycle with appropriate amplitude (not shown). To improve the agreement, the direct and indirect OCS ocean emissions arising from DMS were increased by a factor of 2. These fluxes were chosen as their spatial distribution includes peaks in the Northern Atlantic and Pacific regions. When including the reduction
295 implemented for these terms in the Southern Ocean, the global net increase for direct OCS and indirect OCS from DMS is roughly 10 Gg S yr⁻¹ and 7 Gg S yr⁻¹, respectively, which is relatively small compared to the changes to the vegetative and soil OCS fluxes.

Suntharalingam et al. (2008) recommend a reduction in direct OCS and indirect OCS emissions from DMS by 40% (as this yielded the smallest root-mean-squared error in their analysis) in SH mid-latitude (ML) and high-latitude (HL, here defined as

300 60° – 90°) regions, due to the resulting improvements to the seasonal cycle at Antarctic NOAA-ESRL sites. They also implemented an enhanced OCS tropical ocean source that was aseasonal and uniform across the tropics. However, here we scale up the CS₂ source term to 439 Gg S yr⁻¹ to balance the increased vegetation and soil sink terms discussed above and bring the net budget to near balance. We scaled this flux not necessarily because it was suspected that CS₂ was the erroneous term in the OCS budget, but because it is more realistic to add a flux that is focused spatially over the tropical region already (Kuai et al., 2015). The reason for this geographical distribution is that CS₂ emissions are proportional to temperature and incident solar radiation, hence why the tropics show the strongest emissions (Kettle et al., 2002). Bottom-up estimates of global annual direct and indirect oceanic emissions total approximately 285 – 345 Gg S yr⁻¹ (Lennartz et al., 2017, 2021). Hence, not enough to account for the discrepancy in the global OCS budget. However, for the purposes of this study, we allocate the discrepancy into oceanic emissions, due to the co-location of CS₂ emission fields over the tropics and this is the most suitable representation.

310 Using the flux inventory described here, TOMCAT_{OCS} simulations were carried out covering 2004 to 2018, initialised at 500 ppt in every grid-box and spun up for 10 years between 1994 and 2004. Average yearly burdens for 2004 to 2018 yield a broadly closed OCS budget. Inter-annual variability in meteorology will have an impact on the model's ability to have a mean closed budget over the full time period. The vegetative flux sits roughly in the middle of literature estimates, but the total sink term (1144 Gg S yr⁻¹) is similar to larger estimates from Berry et al. (2013) and Ma et al. (2021), as seen in Table 2, as well as

315 estimates from Glatthor et al. (2015), Kuai et al. (2015) and Launois et al. (2015b), not shown in Table 2. Atmospheric destruction, mainly in the form of tropospheric loss from OH and stratospheric photolysis reactions, account for approximately 154 Gg S yr⁻¹ removal, which is 25% larger than fields used in earlier studies in Table 2, of roughly 126 Gg S yr⁻¹, derived by Watts (2000). The total oceanic emission has been increased by 146% from the starting point of Kettle et al. (2002); the majority of this increase is focused in the tropical region. With a global net annual emission of 1141 Gg S, roughly equal to

320 that of our sink terms, the model yields 14 years of broadly balanced OCS budget, with all terms broadly in line with the findings of recent studies (Berry et al., 2013; Glatthor et al., 2015; Kuai et al., 2015; Launois et al., 2015b; Ma et al., 2021; Remaud et al., 2022). The spatial distribution for the months of January, April, July and October for the adjusted soil uptake and oceanic emissions used in TOMCAT_{OCS} are presented in the supplement: Fig. S6 and S7, respectively.

325 **Table 2.** Global OCS budgets (units Gg S yr⁻¹). Values for past studies are an average of the upper and lower limits stated in those studies unless a value is stated exactly. Values for this study are an average between 2004 and 2018.

Source/Sink Process	Kettle et al. (2002)	Montzka et al. (2007)	Suntharalingham et al. (2008)	Berry et al. ^a (2013)	Ma et al. ^b (2021)	Remaud et al. (2022)	TOMCAT_{OCS} Fluxes
Vegetation	-238	-1115	-490	-738	-1053	-657	-629
Oxic Soil	-130	-127	-120	-355		-236	-322
Reaction with OH	-94	-96		-101	-101	-100	-122
Reaction with O(¹ D)	-11	-11	-130	0	0	0	0
Photolysis	-16	-16		0	-40	0	-32
Ocean	0	0	0	0	0	0	-39
<i>Total Sinks</i>	-489	-1365	-740	-1194	-1194	-993	-1144
Ocean (OCS)	41	40			40		
Ocean (CS ₂)	84		230	876	81	269	689
Ocean (DMS)	154	240			156		
<i>Total Ocean Emission</i>	279	280	230	876	277	269	689
Anthropogenic (OCS)	64	64		64	155		410
Anthropogenic (CS ₂)	116		180	116	188	398	
Anthropogenic (DMS)	1	0		1	6		0
<i>Total Anthropogenic Emission</i>	181	64	180	181	349	398	410
Biomass Burning	38	106	70	136	136	53	42
Other (mainly wetlands & anoxic soils)	26	66	25	0	0	0	0
<i>Total Sources</i>	523	516	505	1193	762	720	1141
<i>Net Budget</i>	34	-849	-235	-2	-432	-273	-3

^aOcean emission term includes an additional photochemical oceanic flux of 600 Gg S.

^bPosterior estimates from the Su inversion are shown here. An ‘unknown’ term is used to quantify a missing source in the inversion and balance their budget.

330 3.4 State-of-the-art Flux Inventory

Emissions used in the TOMCAT_{SOTA} simulation use 5 unique fluxes, which vary monthly, and unlike those used in TOMCAT_{OCS} and TOMCAT_{CON} vary inter-annually. All implemented fluxes are sourced from various bottom-up OCS

inventory studies. The 5 sectors in use here are vegetation and soil uptake, as well as oceanic, anthropogenic and biomass burning emissions. Due to the biomass burning and anthropogenic emissions only being available between 2010 and 2015, 2015 fluxes are repeated through 2016 – 2018. The same is done for 2010 fluxes for the period of 2004 to 2009 for all 5 emission or sink fields.

The sink due to vegetation was derived by implementing the OCS vegetative uptake model from Berry et al. (2013) into the land surface model ORCHIDEE, undertaken and explained in detail by Maignan et al. (2021). Berry et al. (2013) calculate OCS uptake using a series of mechanistically and empirically derived conductances that quantify diffusion of OCS from the boundary layer to leaf stomata, where it is eventually hydrolysed by CA in the leaf cell. Additionally, Maignan et al. (2021) compare the mechanistic model to the LRU-GPP approach, used in the calculation of OCS in Sect. 3.3.1, by running the two in the LMDz6 atmospheric transport model. They found that while the mechanistic approach works better on shorter time and smaller spatial scales, both are suitable for global estimation of vegetative OCS uptake. Preliminary work on implementing a mechanistic soil uptake model, originating from Ogée et al. (2016), into ORCHIDEE was used as the soil flux in this work (Abadie et al., 2022). Calculation of both vegetation and soil uptake, using ORCHIDEE, utilise temporally and spatially varying OCS surface mixing ratios (Remaud et al., 2023), obtained from the TM5 atmospheric transport model, driven by posterior fluxes calculated by Ma et al. (2021). Estimates for each flux are $-532 \text{ Gg S yr}^{-1}$ and $-264 \text{ Gg S yr}^{-1}$ for vegetation and soil, respectively.

Oceanic emissions constitute two parts, direct OCS and indirect CS₂ emissions. Direct OCS is estimated using a global box model and supplemented by measurements of OCS, where the former is developed by von Hobe et al. (2003) and further improves the quantification of the photoproduction rate, parameterization of light-independent production and employs satellite observations of CDOM for use in the model (Lennartz et al., 2017, 2021). Indirect emissions are estimated using CS₂ concentration measurements at the surface and converted using a molar conversion ratio of 0.81 (Chin and Davis, 1993; Lennartz et al., 2017). Biomass burning emissions are estimated by Stinecpher et al. (2019) using the Global Fire Emissions Database, version 4 (GFED4), and scaling CO emissions to OCS. GFED4 utilises six biomass burning categories: savanna and grassland, boreal forests, temperate forests, tropical deforestation and degradation, peatland fires, and agricultural waste burning. Their estimates for the period 1997-2016 total $60 \pm 37 \text{ Gg S yr}^{-1}$. Finally, anthropogenic emissions are from the study by Zumkehr et al. (2018), as described in Sect. 3.3.2, which account for roughly 402 Gg S yr^{-1} of OCS emissions per year.

The spatial distribution for the months of January, April, July, and October (2010 only) for the vegetation and soil uptake and oceanic emissions used in TOMCAT_{SOTA} are presented in the supplement: Fig. S8, S9 and S10, respectively.

4 Results

TOMCAT_{OCS} and TOMCAT_{CON} are compared with NOAA-ESRL surface flask monthly mean measurements and monthly anomalies (monthly mean minus annual mean). TOMCAT_{SOTA} is compared only to monthly anomalies, due to a negative trend in the budget. All 3 models are co-located to the nearest grid box and altitude to the measurements. TOMCAT_{OCS} is also co-

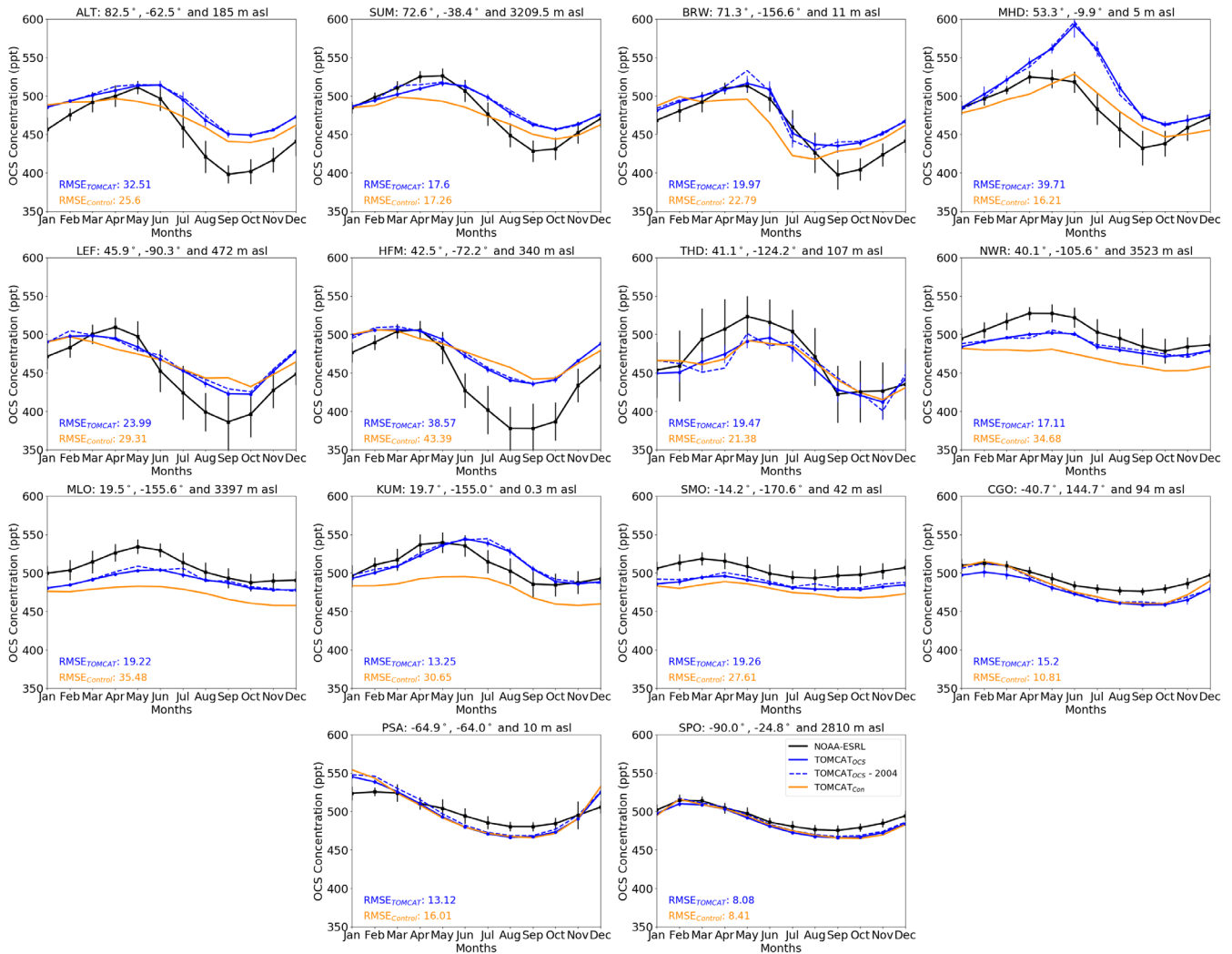
365 located and compared to ACE, which has approximately 98,000 profiles in the modelled time period, all of which are filtered
for outliers before analysis. As ACE measures the upper troposphere and stratosphere primarily, this region is less sensitive to
surface processes, so we only compare TOMCAT_{OCS}. Furthermore, as TOMCAT_{CON} and TOMCAT_{SOTA} have a negative trend,
this makes correcting for bias in both the troposphere and stratosphere and making a comparison throughout the entire profile
challenging. An additional TOMCAT_{OCS} simulation with adjusted atmospheric photolysis for the year 2010 is presented and
370 used to test the suitability of this change to correct a negative model bias in the SH stratosphere.

4.1 Seasonality of Modelled OCS compared to Surface Flask Measurements

TOMCAT simulates OCS distributions down to the surface, where the majority of OCS fluxes occur; it is therefore important
that the model performs well at this level. Figure 1 compares the NOAA-ESRL surface flask measurements (black) with
TOMCAT_{OCS} (solid blue), and TOMCAT_{CON} (orange) simulations. As TOMCAT_{CON} was only run for 2004 (see Sect. 3.1), a
375 blue dashed line representing the year 2004 for TOMCAT_{OCS} is also shown (TOMCAT_{OCS} - 2004). Monthly standard deviation
is calculated for each site and visualised using error bars associated with the observations and TOMCAT_{OCS}. The modelled
vertical layer of TOMCAT_{OCS} and TOMCAT_{CON} closest to the altitude of the measurement site was used for closer comparison
because the bottom-most model layer does not necessarily correspond with the surface due to the relative coarseness of model
grid boxes affecting the simulated surface topography. Figure 2 presents the monthly anomalies for all model runs, including
380 TOMCAT_{SOTA}, as well as the RMSE just for the seasonality (i.e., excluding influence of average concentration), and seasonal
cycle amplitude (SCA) values for all model runs and the surface observations. Therefore, we can dissect the influence of
changes to seasonality influencing RMSE, to some extent. For example, SMO shows a reduction in RMSE from TOMCAT_{CON}
(27.6 ppt) to TOMCAT_{OCS} (19.3 ppt) of 30% in Fig. 1, but also a reduction in RMSE of 28% in Fig. 2. Thus, indicating not
only has TOMCAT_{OCS} improved representation of average concentration, but the seasonality has also improved.

385 Comparisons between TOMCAT_{OCS} and TOMCAT_{CON} are shown in Fig. 1 and Fig. 2 to emphasise the improvements made
by the flux inventory developed in this study, and TOMCAT_{SOTA} to present the latest bottom-up estimates of OCS fluxes.
Generally, there is an improvement in RMSE across all the sites in Fig. 1, but in some cases (MHD and CGO), there is a
degradation. In the case of CGO, this is attributed to an underestimation in average concentration, due to RMSE improving in
Fig. 2, however, at MHD, TOMCAT_{CON} performs better in both RMSE and SCA metrics in both Fig. 1 and Fig. 2.

390 The fluxes used to model TOMCAT_{OCS} reduce the RMSE from an annual mean of 24.3 ppt in TOMCAT_{CON} at all sites to 21.2
ppt (an error reduction of 12.5%) in Fig. 1. This improves to 5.1 ppt (20.4%) if we are to exclude MHD, a particularly poorly
represented site according to this metric. The surface observations show that OCS concentrations peak in April or May in the
NH (ranging from 505 to 540 ppt) and reach a minimum in September or October (ranging from 386 to 488 ppt), which is
consistent in all 10 NH sites and resembles the seasonality of CO₂. Despite several of the NH sites being particularly far north
395 (70 – 90 °N), photosynthesis is still the dominant driving flux, emphasising the strength of the OCS vegetative uptake signal.
Phasing of the seasonal cycle in the SH shifts several months earlier, peaking in February and troughs in August, driven by
the seasonality of oceanic emissions.



400 **Figure 1.** Monthly mean OCS concentration (in ppt) at NOAA-ESRL flask sites (black lines) compared with TOMCAT_{OCS} (solid blue line) for the 2004 to 2018 period. The dashed blue line is just 2004 for the TOMCAT_{OCS} dataset and is compared to TOMCAT_{CON} (orange line). Geographical location of each site is referenced in the titles. Altitude above sea level (asl) of the site is stated and nearest level in TOMCAT used for comparison. Error bars for both NOAA-ESRL and TOMCAT_{OCS} represent standard deviation. Units of RMSE are in ppt.

SCA presented in Fig. 2 show an improvement from a mean absolute difference to the observations of ± 30.5 ppt (39.9%) in
 405 TOMCAT_{CON} and to ± 26.5 ppt (34.8%) in TOMCAT_{OCS}. These metrics suggest that the flux inventory used in TOMCAT_{OCS} offers an improvement in capturing seasonality and observation representation at the surface. The mean absolute difference in SCA of TOMCAT_{SOTA} compared to NOAA-ESRL is ± 43.7 ppt (57.2%).

Relative to the flask measurements, the SCA at the 8 NH continental measurement sites (top 8 plots in Fig. 2) is captured better
 410 by TOMCAT_{OCS} than TOMCAT_{CON}. At all sites there is some improvement in TOMCAT_{OCS} SCA, except for BRW, which shows little change, but an improved RMSE (Fig. 2), and MHD which shows an overestimated SCA by 39.0% in TOMCAT_{OCS}.

SCA is underestimated in TOMCAT_{CON} output at all 8 of these sites by approximately 38.8 ppt on average. TOMCAT_{OCS} improved this disparity to an absolute difference of 36.9 ppt (MHD is overestimated). TOMCAT_{SOTA} shows an absolute difference in SCA to NOAA-ESRL of 45.4 ppt, which improves substantially if LEF and HFM are to be ignored, to 26.9 ppt. Neglecting these same sites for TOMCAT_{OCS} and TOMCAT_{CON}, we see that TOMCAT_{SOTA} shows the best performance in
415 SCA compared to NOAA-ESRL at the continental NH sites.

LEF and HFM are dense woodland sites and have particularly large SCA which can often be a challenge for models to simulate. Here, we show SCAs from TOMCAT_{OCS} of 76 ppt at LEF and 71 ppt at HFM, compared to observed values of 123 ppt and 128 ppt, respectively. The underestimation in TOMCAT_{OCS} could potentially be attributed to using a single value for the LRU parameter globally, as this value is known to vary significantly between plant types (Stimler et al., 2012). The method of
420 estimating OCS uptake using LRU clearly underestimates OCS uptake over dense vegetation, as the model is likely too coarse to include the heavily depleted OCS concentration near the surface. As the GPP product has been compared to a spatially gridded GPP from the FLUXNET network, including Harvard Forest and Park Falls, it is unlikely an underestimation in GPP in this geographical region (Slevin et al., 2016). TOMCAT_{SOTA} underestimates SCA at both sites by approximately 100 ppt, highlighted by RMSE values of 36.1 and 41.2 ppt respectively in Fig. 2.

425 ALT, SUM and BRW are located at high northern latitudes, where the landscape has significantly less vegetation and is more homogeneous than at LEF and HFM, although the seasonal cycle is still driven by typical NH processes. Phasing of the peak and trough of the annual seasonal cycles at ALT, SUM and BRW are improved in TOMCAT_{OCS} output, compared to TOMCAT_{CON}, but RMSE and SCA are not improved significantly in Fig. 2. TOMCAT_{SOTA} improves SCA at ALT, BRW and MHD (9.9 ppt absolute difference to NOAA-ESRL SCA) compared to TOMCAT_{OCS} (39.4 absolute difference to NOAA-
430 ESRL SCA). However, TOMCAT_{SOTA} exhibits larger RMSE values in Fig. 2 due to poor phasing of the seasonality. THD and MHD are both coastal sites and the misalignment in observed and modelled seasonal cycles is attributed to the impact from the ocean fluxes in adjacent model grid boxes. Additionally, capturing the seasonal cycle of trace gases at a site such as MHD can be particularly challenging as there are significant seasonal changes in advected airmasses. Berry et al. (2013) show overestimated peak concentration at MHD in their adjusted flux model runs, but simulations using posterior flux estimates by
435 Ma et al. (2021) show a good alignment at this site, suggesting that the underlying cause is poorly represented surface fluxes. At particularly high-altitude sites, NWR and MLO, Fig. 1 shows that TOMCAT_{OCS} underestimates the average concentration, additionally showing no significant improvement in SCA from TOMCAT_{CON}. The measured SCA at SUM is 98 ppt (428 to 526 ppt), which is modelled relatively poorly by TOMCAT_{CON}, 54.8 ppt, and improved by TOMCAT_{OCS} to 60.1 ppt. A significant difference between SUM and the other two locations is that the topography in the grid boxes for NWR and MLO
440 is very spatially variable; for example, MLO is a high volcano on a relatively small island in the Pacific Ocean. These results suggest the model underestimates OCS concentrations around 1 – 3 km above sea level and there is modest improvement between TOMCAT_{OCS} and TOMCAT_{CON}.

The two NH tropical sites, MLO and KUM, exhibit a seasonal cycle in the measurements similar to that of NH continental sites, with slightly different phasing and a reduced seasonal amplitude, which is due to the influence of oceanic processes.

445 Conversely, SMO, in the SH tropics, is more dominated by ocean processes and peaks earlier in the year. TOMCAT_{OCS} at MLO, KUM and SMO shows varying levels of agreement with the observations. The RMSE in Fig. 1 at KUM is reduced by 56.8% and the SCA is improved compared to TOMCAT_{CON} by 81%, from 17.7 ppt to 3.4 ppt. MLO and SMO average concentration is better represented by TOMCAT_{OCS}, both observing RMSE improvement of -45.8% and -30.2%, respectively. Also note in Fig. 1 that the seasonality is out of phase with the observations, peaking approximately 1 month too late, while
450 KUM is 2 months late. A challenge in diagnosing the misalignment in the Hawaiian sites is their proximity to the ocean, as the $2.8^\circ \times 2.8^\circ$ grid box is dominated by oceanic flux, as are all the boxes around it.

All four SH sites SMO, CGO, PSA and SPO show lower SCA in the observations than all NH sites, ranging from 25 ppt at SMO to 45 ppt at PSA, which is 80% and 65% less variation, respectively, than the forested site HFM. This emphasises the impact vegetation has on NH OCS seasonal cycle. Unlike SMO, the latter 3 sites are dominated much more by oceanic fluxes
455 peaking in SH summer due to the association of phytoplankton growth with OCS emissions, driven by solar radiation. The average concentration of OCS is underestimated by TOMCAT_{OCS} and TOMCAT_{CON} at CGO, PSA and SPO. Seasonal amplitude is overestimated in all models for all three sites. TOMCAT_{OCS} overestimates the SCA at CGO, SPO and PSA, compared to the flask measurements by 5.1 ppt, 6.1 ppt and 33.6 ppt, respectively. In contrast, TOMCAT_{CON} overestimates by 18.2 ppt, 43.2 ppt and 11.8 ppt, respectively. This suggests the reduction in Southern Oceanic emissions in TOMCAT_{OCS}
460 improves seasonality in OCS adequately but could be reduced further. TOMCAT_{SOTA} shows a much larger overestimation in seasonality.

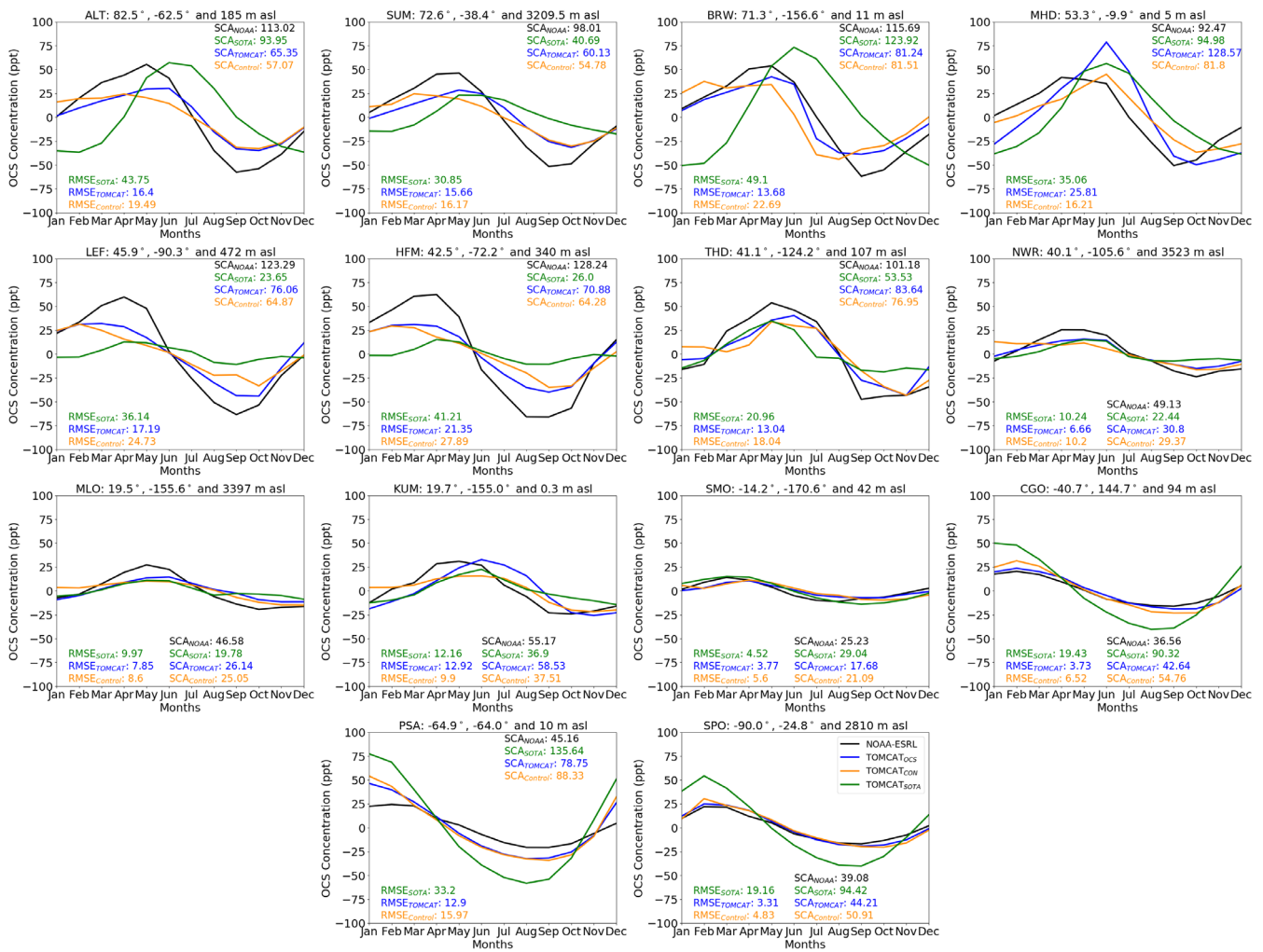
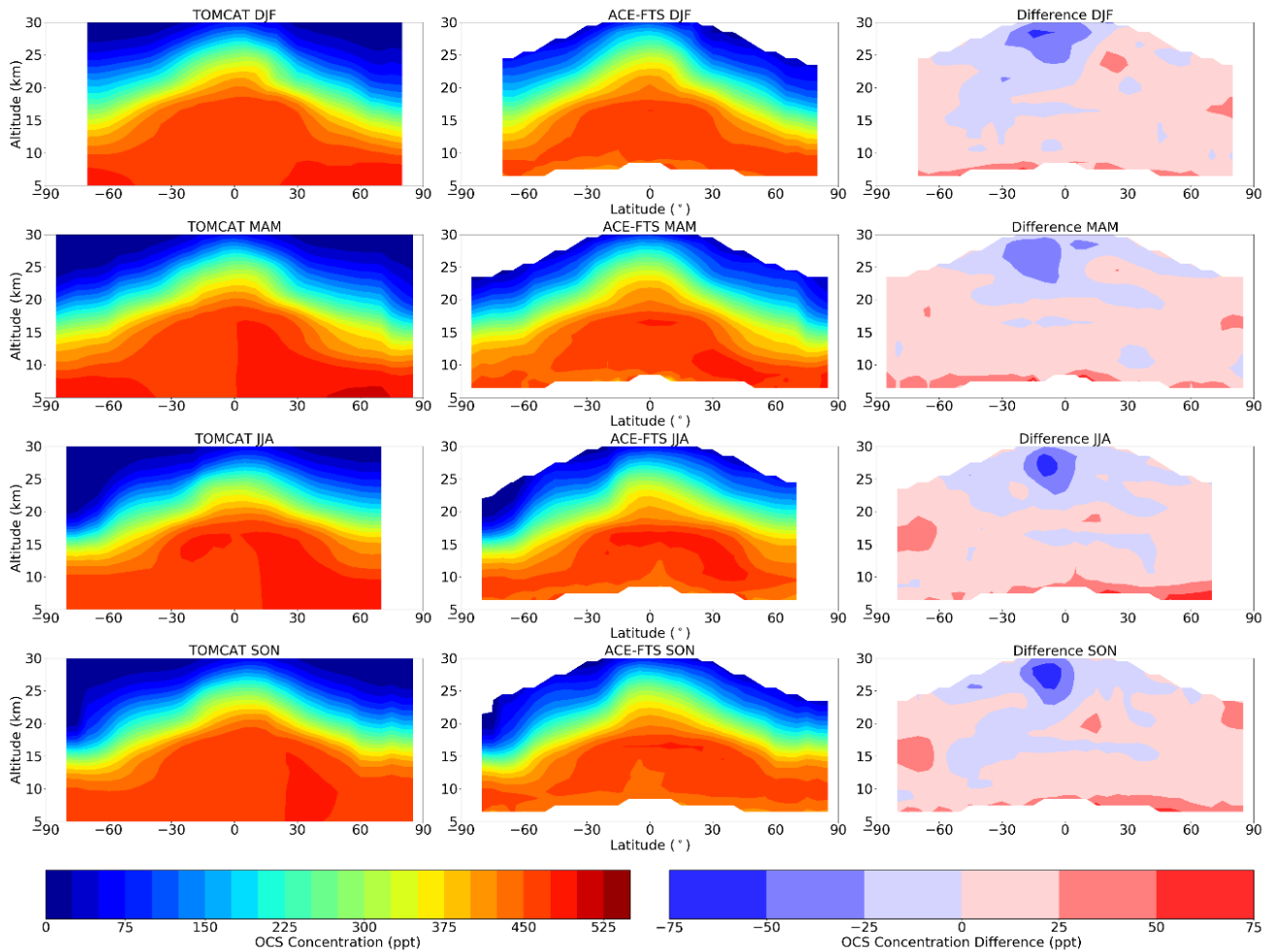


Figure 2. Monthly mean OCS anomalies (monthly mean less annual mean, in ppt) at NOAA-ESRL flask sites (black line) compared with TOMCAT_{OCS} (blue line), TOMCAT_{CON} (orange line) and TOMCAT_{SOTA} (green line) for the 2004 to 2018 period. Geographical location of each site is referenced in the titles. Altitude above sea level (asl) of the site is stated and nearest level in TOMCAT used for comparison. Units of RMSE and SCA are in ppt.

4.2 Spatial Distribution of Modelled OCS compared to Satellite Observations

Figure 3 shows the spatial distribution of atmospheric OCS obtained by averaging ACE profiles across all longitudes and in 5° latitude bins (central column), along with the TOMCAT_{OCS} profiles averaged in the same way (left column). The difference between the two datasets is shown in the right column (TOMCAT_{OCS} minus ACE). ACE-FTS is capable of measuring at altitudes between 6.5 km and 30.5 km, depending on latitude. Figure 3 shows that ACE tropospheric OCS mixing ratios (middle column) range from 425 to 500 ppt, peaking in the upper troposphere-lower stratosphere (UTLS) region, which extends from about 7 km in the NH ML and up to 17 km in the tropics. OCS values decline above and below the UTLS due to removal by vegetation and soil uptake at the surface and photochemistry in the stratosphere, leaving a peak in between which is

475 significantly more prevalent in March – May (MAM) and June – August (JJA). As there is relatively little photosynthesis in
the December – February (DJF) and MAM periods, OCS builds up in the atmosphere, followed by net removal throughout
JJA and September – November (SON). Despite NH photosynthesis beginning slightly before JJA, there is a clear lag in
removing OCS from the upper troposphere. The seasonal peak in OCS in the UTLS region only fully disappears in SON,
480 suggesting there is roughly a 3-month delay on the influence of surface processes on the UTLS ambient mixing ratio. While
this fluctuation is driven by seasonality in photosynthesis, the OCS peak is particularly large and extends lower in the
atmosphere in the NH ML region, co-located with regions of year-round especially large anthropogenic emissions.
The tropopause height is captured adequately by TOMCAT_{OCS} (which is forced by ERA-Interim) and is visible in the
homogeneity of the difference around the UTLS. TOMCAT_{OCS} agrees with ACE to within 25 ppt throughout most of the
troposphere, which is about 5% of the average estimated atmospheric value of OCS (484 ppt) (Montzka et al., 2007). Similar
485 to the seasonal pattern visible in ACE, the tropospheric OCS mixing ratio in TOMCAT_{OCS} peaks before the NH growing
season, MAM. The maximum OCS concentration in TOMCAT_{OCS} can be seen below 6 km (around 50 – 70°N), peaking in
MAM, is larger than maximum OCS observed by ACE, and persists throughout most of the year. The overestimation in the
NH ML is broadly contained within a discrepancy of 25 – 50 ppt from ACE, with the exception of a few anomalies in MAM
and JJA, potentially attributed to underestimated or slower surface OCS uptake, or overestimated anthropogenic emissions in
490 this region. The rate of removal of OCS is not quick enough in JJA to match the measurements exactly. This positive bias in
the model below 10 km in the SH throughout DJF and MAM is probably unrelated to the NH positive model bias and would
likely be resolved by weaker oceanic emission in the SH, despite already having been reduced by 40% (Suntharalingam et al.,
2008).



495 **Figure 3.** Seasonal zonal mean concentration (mixing ratio) of OCS (ppt) from TOMCAT_{OCS} (left), ACE (centre) and the difference between the two (TOMCAT_{OCS} minus ACE, right) for the period of 2004 to 2018. TOMCAT_{OCS} and ACE data averaged in 5-degree latitude bins and over all longitudes.

Differences between the model and observations in the stratosphere are broadly similar to those in the troposphere and are within ± 25 ppt. However, there is considerable model underestimation at 24.5 – 30.5 km between 0° and 30°S, of up to 65 ppt.

500 This region shows a mean seasonal underestimation of between 24.6% and 18.6%, with a peak difference in JJA of 47.5% around 29.5 km at 10°S. As this feature does not follow the pattern of the inter-tropical convergence zone shifting with the hemispheric summertime period, it is unlikely that vertical fluxes are underestimated. The declining gradient in the stratosphere is steeper in the model than in ACE, which suggests that more OCS is being destroyed via photochemical processes in the model than in reality, which we examine in Sect. 4.3.

505 Figure 4 shows TOMCAT_{OCS} profiles (blue) in 30° latitude seasonal bins compared to ACE (red), including the standard deviation (shown as error bars) of ACE at each altitude. It is clear the model replicates the vertical structure of OCS, when

compared to observed OCS profiles from ACE-FTS. The negative discrepancy in the SH tropical stratosphere, visible in Fig. 3 and discussed above, can be seen in the third row of Fig. 4, as TOMCAT_{OCS} deviates from ACE from 20 km up to 30 km. However, as it remains within standard deviation of ACE throughout the entire profile, this suggests the upper atmospheric sinks are modelled moderately well by TOMCAT_{OCS}. This applies to most of the profiles compared in Fig. 4, in that the modelled TOMCAT_{OCS} profiles generally remain within the standard deviation of ACE. The positive model biases in both hemispheres below 10 km in Fig. 3 can be seen in Fig. 4, such that the trend at these altitudes in TOMCAT_{OCS} generally does not match ACE. Between 30°S and 90°N, ACE shows a depletion in OCS towards the surface from as high as 15 km – driven by surface uptake. Where a more neutral or increasing gradient between 90°S and 30°S is seen, as there is minimal vegetative uptake and a seasonal cycle strongly influenced by oceanic emission in this region (see Fig. 1).

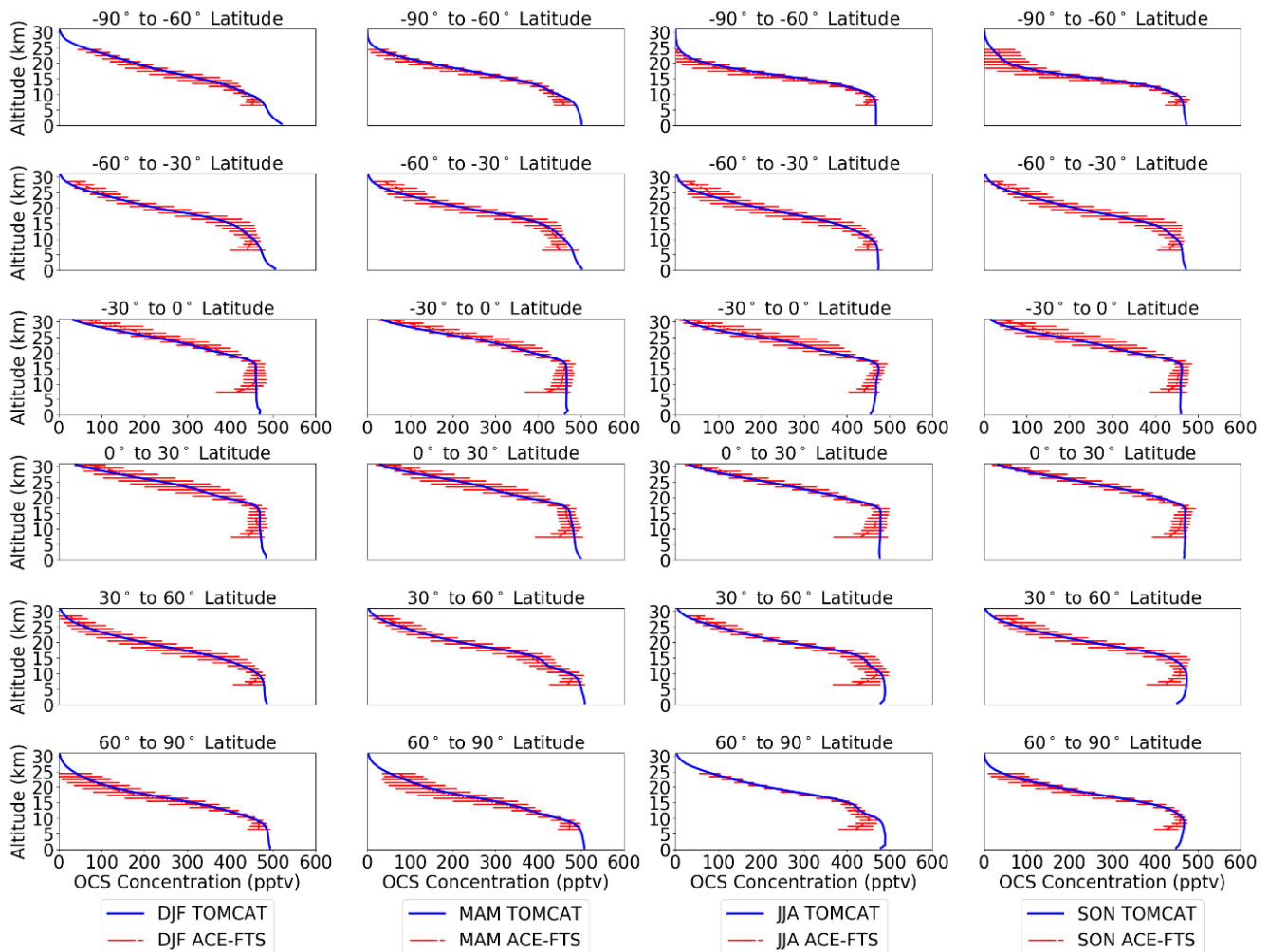


Figure 4. Seasonal mean vertical profiles of OCS concentration (mixing ratio, ppt) from TOMCAT model output (blue) and ACE (red) for six different latitude regions. The error bars are standard deviation of ACE at each altitude level. All profiles are seasonal averages between the years 2004 to 2018.

520 4.3 Modelled OCS using reduced photochemical loss

The TOMCAT_{OCS} model setup described in Sect. 3.1 and 3.3 is used for this experiment in which just the year 2010 is run with an adjusted atmospheric photolysis rate of 75%. The intention of this simulation is to make a simple preliminary assessment of if photolysis alone will correct the underestimation in the SH stratosphere. Figure 5 shows the modified version of TOMCAT_{OCS} on the left, ACE measurements made in 2010 in the middle and the difference between the two (TOMCAT_{OCS} minus ACE). When compared with Fig. 3, the reduced removal of OCS improves the differences between the model and measurements above approximately 20 km, which is to be expected, as this is generally where photolysis is active. The regions that exceed a difference of ± 25 ppt are limited to isolated pockets throughout the year and noticeably more in SON, in the tropics around 20 – 30 km and the SH around the tropopause. Using only a year of data removes a lot of the smoothing we see in Fig. 3, which accounts for some of the differences in Fig. 5. However, there are similar features between the two, specifically persistent (but slightly reduced) underestimation in the model in the tropical SH. We also see an increase in positive model bias, most obviously in the NH between 0 and 30 °N in DJF and SON. Overall, we find that differences between the model and measurements were merely shifted by a 25% reduction in photolysis, introducing biases elsewhere. Further testing, including a simulation using a photolysis rate reduced by 50%, exacerbates these differences further (see Fig. S11), leading to the conclusion that other processes, potentially including transport or convection, require correction to fully resolve these issues in the model.

525
530
535

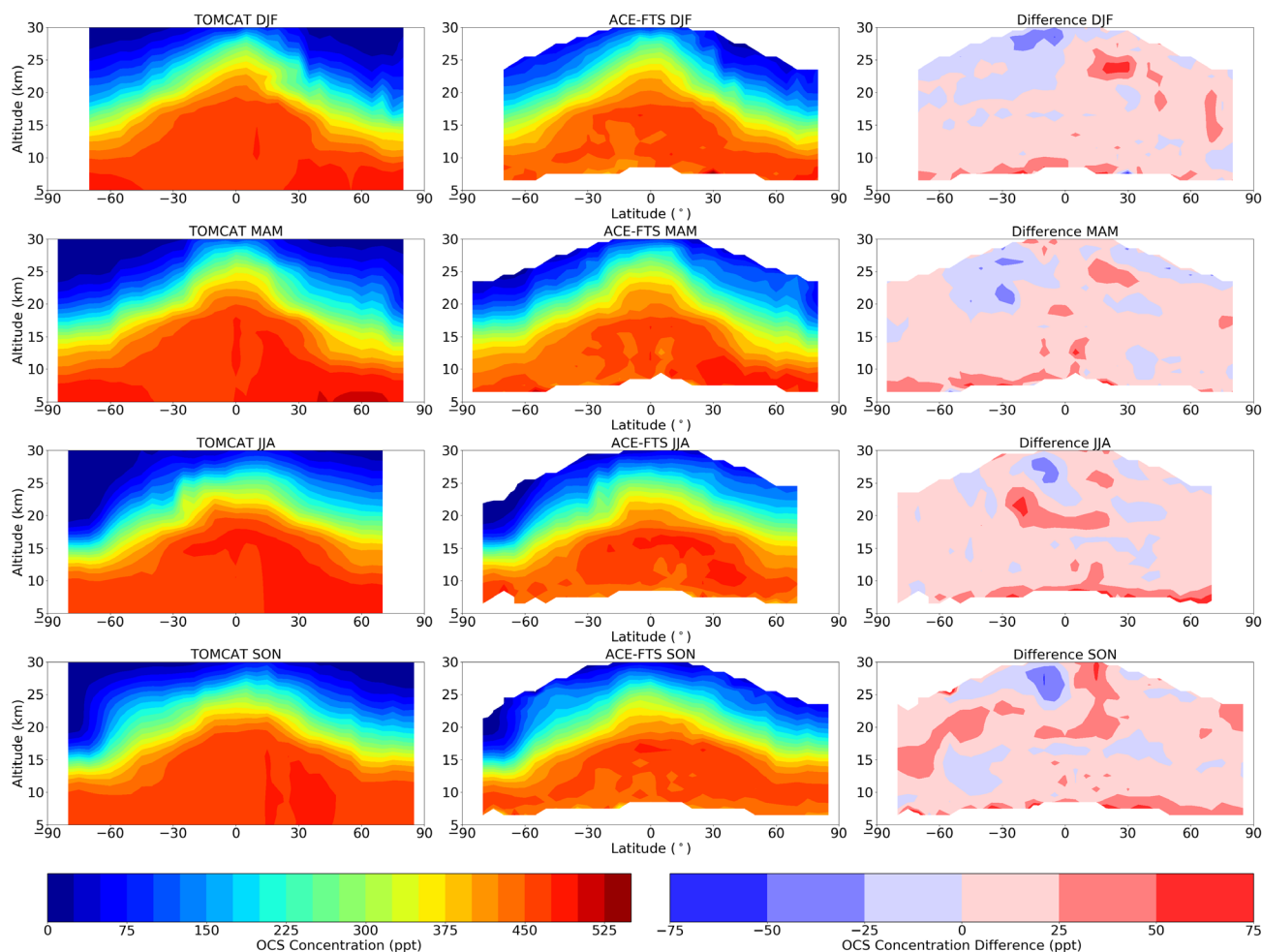


Figure 5. Seasonal zonal mean concentration (mixing ratio) of OCS (ppt) from TOMCAT_{OCS} (left), only for the year 2010 and with a photolysis rate 0.75 times that of TOMCAT_{OCS}, ACE (centre) and the difference between the two (TOMCAT_{OCS} minus ACE, right) for the period of 2004 to 2018. TOMCAT_{OCS} and ACE data averaged in 5-degree latitude bins and over all longitudes.

540 5 Discussion

After a 10-year spin-up period, the TOMCAT_{OCS} simulations of atmospheric OCS concentrations and the vegetative flux, which are dependent on one another in the model, are in equilibrium between 2004 and 2018. By utilizing the LRU-GPP approach, we estimate a mean yearly vegetative OCS uptake of 629 Gg S yr^{-1} , which is within the range and uncertainty of the magnitude of this flux from previous top-down studies (see Table 2). Our estimate is also in the range of recent bottom-up
 545 estimates by Kooijmans et al. (2021), Maignan et al. (2021) and Abadie et al. (2022) ($576 - 756 \text{ Gg S yr}^{-1}$). Our total vegetative and soil sinks agree with findings from Berry et al. (2013) and inversion studies by Kuai et al. (2015), Ma et al. (2021) and Remaud et al. (2022) approximately $\pm 150 \text{ Gg S yr}^{-1}$ (15%). We balance the OCS budget by implementing an enlarged oceanic

CS₂ emission source, for the exclusive reason that it is focused over the tropics (Kettle et al., 2002), rather than it being a flux originating from oxidized CS₂. Bottom-up estimates recommend a constraint on global oceanic emission of OCS to approximately 285 – 350 Gg S yr⁻¹ (Lennartz et al., 2017, 2020, 2021), significantly lower than the fluxes required to balance our budget and thus bringing our tropical ocean estimate into question. It is clear that tropical fluxes are still uncertain, however inverse modelling of OCS fluxes shows that some combination of a larger tropical oceanic source and vegetative sink resolves the budget and produces adequate model comparison with independent observations (Ma et al., 2021; Remaud et al., 2022). TOMCAT_{OCS} output agrees with ACE-FTS profiles of OCS within 25 ppt throughout the majority of the observed atmosphere (approximately 5 km – 30 km), suggesting the sinks in the upper atmosphere are modelled well, with the exception of some discrepancies in the lower troposphere and the tropical lower stratosphere. Photochemical destruction is important in our understanding of atmospheric OCS, and due to photolysis in the stratosphere, the model displays a declining vertical gradient above the tropopause. Our total estimate for this flux is 154 Gg S yr⁻¹, an upward revision of about 40% compared to the previous work of Kettle et al. (2002) and larger than all other estimates in Table 2. Comparison of TOMCAT_{OCS} with ACE profiles shows a good representation of the free troposphere, suggesting that we have found a suitable balance of fluxes at the surface, the spatial variability of which requires improvement. Overestimation in the NH ML region in JJA and SON suggests that surface emissions could be overestimated or that surface uptake does not initialise quick enough or strong enough to remove OCS from the atmosphere at the start of the growing season.

To assess the OCS surface seasonality modelled by TOMCAT_{OCS} we compare it to 2 other simulations: TOMCAT_{CON} and TOMCAT_{SOTA}. The vegetation, soil and ocean emission fields used to drive these models can be found in the supplementary material. When compared with surface flask observations, we show the OCS budget used to calculate TOMCAT_{OCS} reduces RMSE compared to the control, TOMCAT_{CON}, at most sites by approximately 25%, as much as 57% at KUM, but degrading some RMSE, notably at MHD (see Fig. 1). We also show improvements in RMSE at NH continental sites, especially the forested sites of LEF and HFM, but there is still moderate underestimation in NH vegetative uptake. Comparing RMSE in the monthly anomalies between TOMCAT_{OCS} and TOMCAT_{CON} (see Fig. 2) shows that improved average concentration contributed significantly to improving RMSE in Fig. 1, as TOMCAT_{OCS} improves SCA by only 5% compared to TOMCAT_{CON}.

The Hawaiian sites, MLO and KUM, show significantly improved RMSE with TOMCAT_{OCS}, and some improvement in SCA and phasing, suggesting an enhancement in tropical oceanic emission is reasonable. The lack of OCS measurements in the tropics poses a challenge to both quantifying surface OCS exchange in this region both from a mechanistic perspective and from constraining inverted fluxes (Whelan et al., 2018; Ma et al., 2021; Remaud et al., 2022). While TOMCAT_{OCS} shows an adequate comparison with tropical surface sites and a vertical comparison within the variability of ACE, we acknowledge that no attempt has been made in this work to experiment with reducing tropical surface OCS uptake, which has been suggested as an alternative solution to balance the OCS budget (Ma et al., 2021). Overestimation in TOMCAT_{OCS} SCA at SH sites CGO, PSA and SPO, indicates a reduction in oceanic emissions in this region is necessary, due to the limited continental landmass and associated uptake.

The method of estimating vegetative uptake using the LRU approach does have limitations, such as calculating OCS uptake using a constant LRU value of 1.6, which is not representative of reality. LRU values have shown to vary from approximately 1.0 to 4.0 based on different plant type and atmospheric conditions (Sandoval-Soto et al., 2005; Seibt et al., 2010; Stimler et al., 2010, 2012; Kooijmans et al., 2019). Our estimation of vegetative uptake in this work does not replicate OCS uptake universally and it is unclear if this is due to localised differences in LRU or on the GPP fields themselves. When compared to bottom-up vegetation uptake estimates from the ORCHIDEE model used to drive TOMCAT_{SOTA} (Fig. S8), the LRU approach shows similar spatial distribution, magnitude, and seasonality (Fig. S5). There are notable differences in tropical location and magnitude year-round, i.e., South America in January and Africa in April. These regions should have low impact on seasonality in the mid and high latitudes in the NH. However, despite the similarities in the vegetation fields between the two methods, Fig. 2 still shows considerable differences in seasonality in NH sites. The 2-month delayed phasing at BRW is observed by Remaud et al. (2023) in their inter-model comparison study that employs state-of-the-art bottom-up fluxes, similar to those used in this work, and in some cases the same. They attribute this difference to overestimation in NH ocean sources and/or underestimation in vegetative uptake. This agrees with the results of inversion studies by Ma et al. (2021) and Remaud et al. (2022), such that both inversions show increased uptake/decreased emissions of OCS in the NH mid to high latitudes in their posterior fluxes. However, we still lack an explanation for the poor seasonality at the forested sites of LEF and HFM in TOMCAT_{SOTA} (underestimated by approximately 100 ppt at both sites versus the SCA in NOAA measurements). Modelling of OCS and comparing a mechanistic approach and the LRU method in ORCHIDEE, by Maignan et al. (2021) shows that they should behave similarly on a global and seasonal scale. But further work is required to better understand the relationship between OCS uptake and GPP, and why the fluxes driving TOMCAT_{SOTA} do not capture the seasonality of OCS surface mixing ratios.

While soil uptake has been scaled appropriately according to the literature, the distribution is based on work by Kettle et al. (2002) and has since been updated, for example by Abadie et al. (2022). Comparing soil uptake used in TOMCAT_{OCS} vs. TOMCAT_{SOTA} (Fig. S6 vs. S9), the latter is estimated using ORCHIDEE, we see considerable differences which account for the different seasonal cycles in the NH in part, particularly ALT, SUM, BRW and MHD. Figure S9 shows reasonably homogeneous distribution and seasonality compared to S6, which shows far more annual variability and spatial variation.

6 Conclusions

A 3-D chemical transport model was used to compare three OCS flux scenarios; one utilising the LRU approach to quantify vegetative uptake and a series of scaled fluxes (TOMCAT_{OCS}), and two using bottom-up fluxes originating from the literature (TOMCAT_{CON} and TOMCAT_{SOTA}). TOMCAT_{CON} uses fluxes estimated by Kettle et al. (2002) and TOMCAT_{SOTA} uses a series of novel fluxes from recent literature (Lennartz et al., 2017; Zumkehr et al., 2018; Stinecipher et al., 2019; Lennartz et al., 2020; Maignan et al., 2021). All simulations are compared with surface anomalies from the NOAA-ESRL flask network and TOMCAT_{OCS} is compared to ACE-FTS satellite observations. This study is novel in the extended time period analysed

and the quality of vertical comparison with the most recently available ACE-FTS satellite measurements (version 4.1).
615 Furthermore, we see good comparisons with ACE-FTS throughout most of the atmosphere, which suggests the free troposphere
and gradient above the UTLS is well represented by TOMCAT_{OCS}. Therefore, there is a suitable balance between model
sources and sinks from the surface to simulate atmospheric OCS. Future application of the TOMCAT_{OCS} model could
encompass its use in comparison with and interpretation of nadir viewing satellite observations, for example from the Infrared
Sounding Interferometer (IASI) instruments.

620 TOMCAT_{OCS} and TOMCAT_{CON} surface concentration is compared, and the former is shown to reduce root mean square error
(RMSE) compared to 14 NOAA-ESRL by 12.5% across all 14 sites, up to 20% when neglecting MHD. Further, surface
anomalies (monthly mean minus annual mean) are compared between all three model runs, yielding a RMSE that removes
annual mean and focuses solely on seasonality. TOMCAT_{OCS} reduces the RMSE in the anomalies by 18.7% and 52.4%
625 compared to TOMCAT_{CON} and TOMCAT_{SOTA}, respectively. Adequately modelling seasonality globally proved to be a
challenge and while TOMCAT_{OCS} performed best relative to NOAA-ESRL flask observations, the seasonal cycle amplitude
was misaligned by a mean absolute amount of 26.6 ppt by TOMCAT_{OCS} and by 43.7 ppt by TOMCAT_{SOTA}. We have shown
that the LRU approach for quantifying vegetative uptake yields similar annual estimates (629 Gg S yr⁻¹) to mechanistic and
inversion approaches (657 – 756 Gg S yr⁻¹) and resembles spatial variability (Maignan et al., 2021; Remaud et al., 2022). To
630 suitably estimate a total biosphere uptake that reflects recent inversion studies, of roughly 893 – 1053 Gg S yr⁻¹ (Remaud et
al., 2022; Ma et al., 2021), soil uptake is uplifted to by 2.5 times, yielding a combined total of 951 Gg S yr⁻¹. To bring the
budget into balance we increase total net oceanic emissions to 650 Gg S yr⁻¹, from the starting point of 279 Gg S yr⁻¹ (Kettle
et al., 2002). Overall, we draw similar conclusions to other works, that the tropics are a likely location for a compensatory
source of OCS.

Here, we make recommendations for advancing this work. The following changes are necessary in the future to improve the
635 GPP-LRU approach such as: using inter-annually varying GPP and CO₂ mixing ratios, and a temporally and spatially resolved
LRU. It is challenging to achieve at a high resolution LRU product on a global scale, however, plant-functional-type-dependent
datasets of LRU are available (Seibt et al., 2010; Whelan et al., 2018; Maignan et al., 2021), hence an initial step would be just
to vary LRU based on ecosystem on a continental or ecosystem scale. Advances are being made in this area, with mechanistic
and LRU approaches emerging that reduce uncertainty in OCS vegetative uptake (Kooijmans et al., 2021; Maignan et al.,
640 2021). The use of an enhanced tropical ocean source to balance the budget is justified in this work by offering suitable satellite
and surface observational comparisons. However, we acknowledge that oceanic emissions alone may not account for this
discrepancy and based on TOMCAT_{OCS} performance at MLO and KUM, this is not a perfect solution for balancing the global
OCS budget.

While optimised fluxes from inversion studies show the most up-to-date distribution of OCS fluxes at the surface, what they
645 lack is information on bottom-up processes. As we have seen in Fig. 2, TOMCAT_{SOTA} lacks suitable seasonality, in terms of
both SCA and phasing, for many NH surface measurement sites. More work is required to dissect the impact of individual

fluxes on seasonality and further understand why bottom-up fluxes differ so greatly from posterior inverted fluxes, most importantly vegetative uptake and oceanic emissions.

650 While we have shown that TOMCAT_{OCS} compares well with satellite observations, the region between the surface and approximately 6 km, which is not measured by ACE-FTS, could hold a lot of information useful in resolving surface fluxes. Measurements at the surface are sensitive to minor flux changes, although in the well-mixed mid to upper troposphere these spatial changes are less important. Validation of model output to ground-based Fourier Transform spectrometer column OCS measurements could improve our understanding and ability to model the lower troposphere. Furthermore, incorporating measurements with vertical information into an inversion scheme has been shown to improve the posterior OCS fluxes, 655 specifically using HIPPO flight data (Ma et al., 2021). Therefore, further study following on from this work will be to derive an a posteriori set of fluxes using an inversion scheme based on an up-to-date prior, using surface observations and a dataset containing vertical information near the surface.

Code and Data Availability

Anthropogenic OCS emission data are available at <https://portal.nersc.gov/project/m2319/> (Campbell, 2022; Zumkehr et al., 660 2018). GPP dataset is available at <https://datashare.ed.ac.uk/handle/10283/2080> (Slevin et al., 2016). ACE-FTS data are available at <http://www.ace.uwaterloo.ca/data.php> (ACE-FTS, 2022). NOAA-ESRL surface flask measurements of OCS are available at <https://www.esrl.noaa.gov/gmd/dv/data/> (ESRL Global Monitoring Laboratory, 2022). Model data are available at <https://doi.org/10.5281/zenodo.6368542>.

Author Contribution

665 Model runs and data analysis were performed by MPCar, with support from RJP. JJH and MPChi designed the study. CJW provided the CO₂ model data. Control OCS emissions were provided by PS. TOMCAT model is maintained and updated by the team at the University of Leeds: MPChi, WF, CW and RJP. Manuscript was written by MPCar, with contributions from all co-authors.

Competing Interests

670 The authors declare that they have no conflict of interest.

Acknowledgements

Computation and data analysis were carried out on the ARC computing system at Leeds and the ALICE/SPECTRE system at Leicester. The authors thank P. Bernath for access to ACE-FTS satellite observations, D. Slevin, S. Tett and M. Williams for

access to GPP data from JULES and S. Montzka and J. Elkins and other contributors from NOAA for providing the flask
675 measurements. The authors thank M. Remaud, J. Ma, M. Krol and all other principal contributors to the TRANSCOM inter-
model comparison study for providing gridded fluxes used in the TOMCAT_{SOTA} simulations.

Financial support

MPCar thanks the Leicester Institute of Space and Earth Observation, for providing a studentship at the University of Leicester.
This study was funded as part of the UK Research and Innovation Natural Environment Research Council's support of the
680 National Centre for Earth Observation, contract number PR140015.

References

- Abadie, C., Maignan, F., Remaud, M., Ogée, J., Campbell, J. E., Whelan, M. E., Kitz, F., Spielmann, F. M., Wohlfahrt, G.,
Wehr, R., Sun, W., Raoult, N., Seibt, U., Hauglustaine, D., Lennartz, S. T., Belviso, S., Montagne, D., and Peylin, P.: Global
modelling of soil carbonyl sulfide exchanges, *Biogeosciences*, 19, 2427–2463, <https://doi.org/10.5194/bg-19-2427-2022>,
685 2022.
- ESRL Global Monitoring Laboratory - FTP Navigator: <https://gml.noaa.gov/dv/data/>, last access: 14 March 2022.
- Asaf, D., Rotenberg, E., Tatarinov, F., Dicken, U., Montzka, S. A., and Yakir, D.: Ecosystem photosynthesis inferred from
measurements of carbonyl sulphide flux, *Nat. Geosci.*, 6, 186–190, <https://doi.org/10.1038/ngeo1730>, 2013.
- Aydin, M., Britten, G. L., Montzka, S. A., Buizert, C., Primeau, F., Petrenko, V., Battle, M. B., Nicewonger, M. R., Patterson,
690 J., Hmiel, B., and Saltzman, E. S.: Anthropogenic Impacts on Atmospheric Carbonyl Sulfide Since the 19th Century Inferred
From Polar Firm Air and Ice Core Measurements, *Journal of Geophysical Research: Atmospheres*, 125, e2020JD033074,
<https://doi.org/10.1029/2020JD033074>, 2020.
- Barkley, M. P., Palmer, P. I., Boone, C. D., Bernath, P. F., and Suntharalingam, P.: Global distributions of carbonyl sulfide in
the upper troposphere and stratosphere, *Geophys. Res. Lett.*, 35, L14810, <https://doi.org/10.1029/2008GL034270>, 2008.
- 695 Barnes, I., Becker, K. H., and Patroescu, I.: The tropospheric oxidation of dimethyl sulfide: A new source of carbonyl sulfide,
Geophysical Research Letters, 21, 2389–2392, <https://doi.org/10.1029/94GL02499>, 1994.
- Bernath, P. F.: The Atmospheric Chemistry Experiment (ACE), *J. Quant. Spectrosc. Radiat. Transfer*, 186, 3–16,
<https://doi.org/10.1016/j.jqsrt.2016.04.006>, 2017.
- Bernath, P. F., McElroy, C. T., Abrams, M. C., Boone, C. D., Butler, M., Camy-Peyret, C., Carleer, M., Clerbaux, C., Coheur,
700 P.-F., Colin, R., DeCola, P., DeMazière, M., Drummond, J. R., Dufour, D., Evans, W. F. J., Fast, H., Fussen, D., Gilbert, K.,
Jennings, D. E., Llewellyn, E. J., Lowe, R. P., Mahieu, E., McConnell, J. C., McHugh, M., McLeod, S. D., Michaud, R.,
Midwinter, C., Nassar, R., Nichitiu, F., Nowlan, C., Rinsland, C. P., Rochon, Y. J., Rowlands, N., Semeniuk, K., Simon, P.,
Skelton, R., Sloan, J. J., Soucy, M.-A., Strong, K., Tremblay, P., Turnbull, D., Walker, K. A., Walkty, I., Wardle, D. A.,

- Wehrle, V., Zander, R., and Zou, J.: Atmospheric Chemistry Experiment (ACE): Mission overview, *Geophysical Research Letters*, 32, <https://doi.org/10.1029/2005GL022386>, 2005.
- Berry, J., Wolf, A., Campbell, J. E., Baker, I., Blake, N., Blake, D., Denning, A. S., Kawa, S. R., Montzka, S. A., Seibt, U., Stimler, K., Yakir, D., and Zhu, Z.: A coupled model of the global cycles of carbonyl sulfide and CO₂: A possible new window on the carbon cycle, *J. Geophys. Res. Biogeosci.*, 118, 842–852, <https://doi.org/10.1002/jgrg.20068>, 2013.
- Blonquist, J. M., Montzka, S. A., Munger, J. W., Yakir, D., Desai, A. R., Dragoni, D., Griffis, T. J., Monson, R. K., Scott, R. L., and Bowling, D. R.: The potential of carbonyl sulfide as a proxy for gross primary production at flux tower sites, *Journal of Geophysical Research: Biogeosciences*, 116, <https://doi.org/10.1029/2011JG001723>, 2011.
- Boone, C. D. and Bernath, P. F.: The instrumental line shape of the atmospheric chemistry experiment Fourier transform spectrometer (ACE-FTS), *Journal of Quantitative Spectroscopy and Radiative Transfer*, 230, 1–12, <https://doi.org/10.1016/j.jqsrt.2019.03.018>, 2019.
- Boone, C. D., Bernath, P. F., Cok, D., Jones, S. C., and Steffen, J.: Version 4 retrievals for the atmospheric chemistry experiment Fourier transform spectrometer (ACE-FTS) and imagers, *Journal of Quantitative Spectroscopy and Radiative Transfer*, 247, 106939, <https://doi.org/10.1016/j.jqsrt.2020.106939>, 2020.
- Campbell, J. E., Carmichael, G. R., Chai, T., Mena-Carrasco, M., Tang, Y., Blake, D. R., Blake, N. J., Vay, S. A., Collatz, G. J., Baker, I., Berry, J. A., Montzka, S. A., Sweeney, C., Schnoor, J. L., and Stanier, C. O.: Photosynthetic Control of Atmospheric Carbonyl Sulfide During the Growing Season, *Sci.*, 322, 1085–1088, <https://doi.org/10.1126/science.1164015>, 2008.
- Chen, M., Rafique, R., Asrar, G. R., Bond-Lamberty, B., Ciais, P., Zhao, F., Reyer, C. P. O., Ostberg, S., Chang, J., Ito, A., Yang, J., Zeng, N., Kalnay, E., West, T., Leng, G., Francois, L., Munhoven, G., Henrot, A., Tian, H., Pan, S., Nishina, K., Viovy, N., Morfopoulos, C., Betts, R., Schaphoff, S., Steinkamp, J., and Hickler, T.: Regional contribution to variability and trends of global gross primary productivity, *Environ. Res. Lett.*, 12, 105005, <https://doi.org/10.1088/1748-9326/aa8978>, 2017.
- Chin, M. and Davis, D., D.: Global sources and sinks of OCS and CS₂ and their distributions, *Global Biogeochem. Cycles*, 7, 321–337, <https://doi.org/10.1029/93GB00568>, 1993.
- Chipperfield, M. P.: New version of the TOMCAT/SLIMCAT off-line chemical transport model: Intercomparison of stratospheric tracer experiments, *Quarterly Journal of the Royal Meteorological Society*, 132, 1179–1203, <https://doi.org/10.1256/qj.05.51>, 2006.
- Claxton, T., Hossaini, R., Wild, O., Chipperfield, M. P., and Wilson, C.: On the Regional and Seasonal Ozone Depletion Potential of Chlorinated Very Short-Lived Substances, *Geophysical Research Letters*, 46, 5489–5498, <https://doi.org/10.1029/2018GL081455>, 2019.
- Crutzen, P. J.: The possible importance of CSO for the sulfate layer of the stratosphere, *Geophys. Res. Lett.*, 3, 73–76, <https://doi.org/10.1029/GL003i002p000073>, 1976.
- Dee, D. P., Uppala, S. M., Simmons, A. J., Berrisford, P., Poli, P., Kobayashi, S., Andrae, U., Balmaseda, M. A., Balsamo, G., Bauer, P., Bechtold, P., Beljaars, A. C. M., Berg, L. van de, Bidlot, J., Bormann, N., Delsol, C., Dragani, R., Fuentes, M.,

- Geer, A. J., Haimberger, L., Healy, S. B., Hersbach, H., Hólm, E. V., Isaksen, L., Kállberg, P., Köhler, M., Matricardi, M., McNally, A. P., Monge-Sanz, B. M., Morcrette, J.-J., Park, B.-K., Peubey, C., Rosnay, P. de, Tavolato, C., Thépaut, J.-N., and Vitart, F.: The ERA-Interim reanalysis: configuration and performance of the data assimilation system, *Quarterly Journal of the Royal Meteorological Society*, 137, 553–597, <https://doi.org/10.1002/qj.828>, 2011.
- Duncan, B. N., Martin, R. V., Staudt, A. C., Yevich, R., and Logan, J. A.: Interannual and seasonal variability of biomass burning emissions constrained by satellite observations, *Journal of Geophysical Research: Atmospheres*, 108, ACH 1-1-ACH 1-22, <https://doi.org/10.1029/2002JD002378>, 2003.
- Feng, W., Chipperfield, M. P., Dhomse, S., Monge-Sanz, B. M., Yang, X., Zhang, K., and Ramonet, M.: Evaluation of cloud convection and tracer transport in a three-dimensional chemical transport model, *Atmos. Chem. Phys.*, 21, 2011.
- Fung, I. Y., Tucker, C. J., and Prentice, K. C.: Application of Advanced Very High Resolution Radiometer vegetation index to study atmosphere-biosphere exchange of CO₂, *Journal of Geophysical Research: Atmospheres*, 92, 2999–3015, <https://doi.org/10.1029/JD092iD03p02999>, 1987.
- Glatthor, N., Höpfner, M., Baker, I. T., Berry, J., Campbell, J. E., Kawa, S. R., Krysztofiak, G., Leyser, A., Sinnhuber, B.-M., Stiller, G. P., Stinecipher, J., and Clarmann, T. von: Tropical sources and sinks of carbonyl sulfide observed from space, *Geophys. Res. Lett.*, 42, 10,082-10,090, <https://doi.org/10.1002/2015GL066293>, 2015.
- Glatthor, N., Höpfner, M., Leyser, A., Stiller, G. P., von Clarmann, T., Grabowski, U., Kellmann, S., Linden, A., Sinnhuber, B.-M., Krysztofiak, G., and Walker, K. A.: Global carbonyl sulfide (OCS) measured by MIPAS/Envisat during 2002–2012, *Atmos. Chem. Phys.*, 17, 2631–2652, <https://doi.org/10.5194/acp-17-2631-2017>, 2017.
- Gloor, E., Wilson, C., Chipperfield, M. P., Chevallier, F., Buermann, W., Boesch, H., Parker, R., Somkuti, P., Gatti, L. V., Correia, C., Domingues, L. G., Peters, W., Miller, J., Deeter, M. N., and Sullivan, M. J. P.: Tropical land carbon cycle responses to 2015/16 El Niño as recorded by atmospheric greenhouse gas and remote sensing data, *Philosophical Transactions of the Royal Society B: Biological Sciences*, 373, 20170302, <https://doi.org/10.1098/rstb.2017.0302>, 2018.
- Gordon, I. E., Rothman, L. S., Hill, C., Kochanov, R. V., Tan, Y., Bernath, P. F., Birk, M., Boudon, V., Campargue, A., Chance, K. V., Drouin, B. J., Flaud, J.-M., Gamache, R. R., Hodges, J. T., Jacquemart, D., Perevalov, V. I., Perrin, A., Shine, K. P., Smith, M.-A. H., Tennyson, J., Toon, G. C., Tran, H., Tyuterev, V. G., Barbe, A., Császár, A. G., Devi, V. M., Furtenbacher, T., Harrison, J. J., Hartmann, J.-M., Jolly, A., Johnson, T. J., Karman, T., Kleiner, I., Kyuberis, A. A., Loos, J., Lyulin, O. M., Massie, S. T., Mikhailenko, S. N., Moazzen-Ahmadi, N., Müller, H. S. P., Naumenko, O. V., Nikitin, A. V., Polyansky, O. L., Rey, M., Rotger, M., Sharpe, S. W., Sung, K., Starikova, E., Tashkun, S. A., Auwera, J. V., Wagner, G., Wilzewski, J., Wcisło, P., Yu, S., and Zak, E. J.: The HITRAN2016 molecular spectroscopic database, *Journal of Quantitative Spectroscopy and Radiative Transfer*, 203, 3–69, <https://doi.org/10.1016/j.jqsrt.2017.06.038>, 2017.
- Hannigan, J. W., Ortega, I., Shams, S. B., Blumenstock, T., Campbell, J. E., Conway, S., Flood, V., Garcia, O., Griffith, D., Grutter, M., Hase, F., Jeseck, P., Jones, N., Mahieu, E., Makarova, M., De Mazière, M., Morino, I., Murata, I., Nagahama, T., Nakijima, H., Notholt, J., Palm, M., Poberovskii, A., Rettinger, M., Robinson, J., Röhlings, A. N., Schneider, M., Servais, C., Smale, D., Stremme, W., Strong, K., Sussmann, R., Te, Y., Vigouroux, C., and Wizenberg, T.: Global Atmospheric OCS

- Trend Analysis From 22 NDACC Stations, *Journal of Geophysical Research: Atmospheres*, 127, e2021JD035764, <https://doi.org/10.1029/2021JD035764>, 2022.
- Hilton, T. W., Whelan, M. E., Zumkehr, A., Kulkarni, S., Berry, J. A., Baker, I. T., Montzka, S. A., Sweeney, C., Miller, B.
775 R., and Elliott Campbell, J.: Peak growing season gross uptake of carbon in North America is largest in the Midwest USA, *Nature Climate Change*, 7, 450–454, <https://doi.org/10.1038/nclimate3272>, 2017.
- von Hobe, M., Najjar, R. G., Kettle, A. J., and Andreae, M. O.: Photochemical and physical modeling of carbonyl sulfide in the ocean, *Journal of Geophysical Research: Oceans*, 108, <https://doi.org/10.1029/2000JC000712>, 2003.
- Huijnen, V., Williams, J., van Weele, M., van Noije, T., Krol, M., Dentener, F., Segers, A., Houweling, S., Peters, W., de Laat,
780 J., Boersma, F., Bergamaschi, P., van Velthoven, P., Le Sager, P., Eskes, H., Alkemade, F., Scheele, R., Nédélec, P., and Pätz, H.-W.: The global chemistry transport model TM5: description and evaluation of the tropospheric chemistry version 3.0, *Geoscientific Model Development*, 3, 445–473, <https://doi.org/10.5194/gmd-3-445-2010>, 2010.
- Kato, H., Saito, M., Nagahata, Y., and Katayama, Y.: Degradation of ambient carbonyl sulfide by *Mycobacterium* spp. in soil, *Microbiology*, 154, 249–255, <https://doi.org/10.1099/mic.0.2007/011213-0>, 2008.
- 785 Kesselmeier, J., Teusch, N., and Kuhn, U.: Controlling variables for the uptake of atmospheric carbonyl sulfide by soil, *Journal of Geophysical Research: Atmospheres*, 104, 11577–11584, <https://doi.org/10.1029/1999JD900090>, 1999.
- Kettle, A. J. and Andreae, M. O.: Flux of dimethylsulfide from the oceans: A comparison of updated data sets and flux models, *Journal of Geophysical Research: Atmospheres*, 105, 26793–26808, <https://doi.org/10.1029/2000JD900252>, 2000.
- Kettle, A. J., Kuhn, U., Hobe, M. von, Kesselmeier, J., and Andreae, M. O.: Global budget of atmospheric carbonyl sulfide:
790 Temporal and spatial variations of the dominant sources and sinks, *J. Geophys. Res.*, 107, ACH 25-1-ACH 25-16, <https://doi.org/10.1029/2002JD002187>, 2002.
- Kitz, F., Spielmann, F. M., Hammerle, A., Kolle, O., Migliavacca, M., Moreno, G., Ibrom, A., Krasnov, D., Noe, S. M., and Wohlfahrt, G.: Soil COS Exchange: A Comparison of Three European Ecosystems, *Global Biogeochemical Cycles*, 34, e2019GB006202, <https://doi.org/10.1029/2019GB006202>, 2020.
- 795 Kooijmans, L. M. J., Sun, W., Aalto, J., Erkkilä, K.-M., Maseyk, K., Seibt, U., Vesala, T., Mammarella, I., and Chen, H.: Influences of light and humidity on carbonyl sulfide-based estimates of photosynthesis, *Proceedings of the National Academy of Sciences*, 116, 2470–2475, <https://doi.org/10.1073/pnas.1807600116>, 2019.
- Kooijmans, L. M. J., Cho, A., Ma, J., Kaushik, A., Haynes, K. D., Baker, I., Lujikx, I. T., Groenink, M., Peters, W., Miller, J. B., Berry, J. A., Ogée, J., Meredith, L. K., Sun, W., Kohonen, K.-M., Vesala, T., Mammarella, I., Chen, H., Spielmann, F. M.,
800 Wohlfahrt, G., Berkelhammer, M., Whelan, M. E., Maseyk, K., Seibt, U., Commane, R., Wehr, R., and Krol, M.: Evaluation of carbonyl sulfide biosphere exchange in the Simple Biosphere Model (SiB4), *Biogeosciences*, 18, 6547–6565, <https://doi.org/10.5194/bg-18-6547-2021>, 2021.
- Kremser, S., Jones, N. B., Palm, M., Lejeune, B., Wang, Y., Smale, D., and Deutscher, N. M.: Positive trends in Southern Hemisphere carbonyl sulfide, *Geophys. Res. Lett.*, 42, 9473–9480, <https://doi.org/10.1002/2015GL065879>, 2015.

- 805 Kremser, S., Thomason, L. W., Hobe, M. von, Hermann, M., Deshler, T., Timmreck, C., Toohey, M., Stenke, A., Schwarz, J. P., Weigel, R., Fueglistaler, S., Prata, F. J., Vernier, J.-P., Schlager, H., Barnes, J. E., Antuña-Marrero, J.-C., Fairlie, D., Palm, M., Mahieu, E., Notholt, J., Rex, M., Bingen, C., Vanhellefont, F., Bourassa, A., Plane, J. M. C., Klocke, D., Carn, S. A., Clarisse, L., Trickl, T., Neely, R., James, A. D., Rieger, L., Wilson, J. C., and Meland, B.: Stratospheric aerosol—Observations, processes, and impact on climate, *Reviews of Geophysics*, 54, 278–335, <https://doi.org/10.1002/2015RG000511>, 2016.
- 810 Kuai, L., Worden, J. R., Campbell, J. E., Kulawik, S. S., Li, K.-F., Lee, M., Weidner, R. J., Montzka, S. A., Moore, F. L., Berry, J. A., Baker, I., Denning, A. S., Bian, H., Bowman, K. W., Liu, J., and Yung, Y. L.: Estimate of carbonyl sulfide tropical oceanic surface fluxes using Aura Tropospheric Emission Spectrometer observations, *J. Geophys. Res. Atmos.*, 120, 11,012–11,023, <https://doi.org/10.1002/2015JD023493>, 2015.
- Launois, T., Belviso, S., Bopp, L., Fichot, C. G., and Peylin, P.: A new model for the global biogeochemical cycle of carbonyl sulfide - Part 1: Assessment of direct marine emissions with an oceanic general circulation and biogeochemistry model, *Atmospheric Chemistry and Physics*, 15, 2295–2312, <https://doi.org/10.5194/acp-15-2295-2015>, 2015a.
- 815 Launois, T., Peylin, P., Belviso, S., and Poulter, B.: A new model of the global biogeochemical cycle of carbonyl sulfide – Part 2: Use of carbonyl sulfide to constrain gross primary productivity in current vegetation models, *Atmospheric Chemistry and Physics*, 15, 9285–9312, <https://doi.org/10.5194/acp-15-9285-2015>, 2015b.
- 820 Lejeune, B., Mahieu, E., Vollmer, M. K., Reimann, S., Bernath, P. F., Boone, C. D., Walker, K. A., and Servais, C.: Optimized approach to retrieve information on atmospheric carbonyl sulfide (OCS) above the Jungfraujoch station and change in its abundance since 1995, *Journal of Quantitative Spectroscopy and Radiative Transfer*, 186, 81–95, <https://doi.org/10.1016/j.jqsrt.2016.06.001>, 2017.
- Lennartz, S. T., Marandino, C. A., von Hobe, M., Cortes, P., Quack, B., Simo, R., Booge, D., Pozzer, A., Steinhoff, T., Arevalo-Martinez, D. L., Kloss, C., Bracher, A., Röttgers, R., Atlas, E., and Krüger, K.: Direct oceanic emissions unlikely to account for the missing source of atmospheric carbonyl sulfide, *Atmospheric Chemistry and Physics*, 17, 385–402, <https://doi.org/10.5194/acp-17-385-2017>, 2017.
- Lennartz, S. T., Marandino, C. A., von Hobe, M., Andreae, M. O., Aranami, K., Atlas, E., Berkelhammer, M., Bingemer, H., Booge, D., Cutter, G., Cortes, P., Kremser, S., Law, C. S., Marriner, A., Simó, R., Quack, B., Uher, G., Xie, H., and Xu, X.: 830 Marine carbonyl sulfide (OCS) and carbon disulfide (CS₂): a compilation of measurements in seawater and the marine boundary layer, *Earth System Science Data*, 12, 591–609, <https://doi.org/10.5194/essd-12-591-2020>, 2020.
- Lennartz, S. T., Gauss, M., von Hobe, M., and Marandino, C. A.: Monthly resolved modelled oceanic emissions of carbonyl sulphide and carbon disulphide for the period 2000–2019, *Earth System Science Data*, 13, 2095–2110, <https://doi.org/10.5194/essd-13-2095-2021>, 2021.
- 835 Li, W., Yu, L., Yuan, D., Wu, Y., and Zeng, X.: A study of the activity and ecological significance of carbonic anhydrase from soil and its microbes from different karst ecosystems of Southwest China, *Plant Soil*, 272, 133–141, <https://doi.org/10.1007/s11104-004-4335-9>, 2005.

- Ma, J., Kooijmans, L. M. J., Cho, A., Montzka, S. A., Glatthor, N., Worden, J. R., Kuai, L., Atlas, E. L., and Krol, M. C.: Inverse modelling of carbonyl sulfide: implementation, evaluation and implications for the global budget, *Atmos. Chem. Phys.*, 21, 3507–3529, <https://doi.org/10.5194/acp-21-3507-2021>, 2021.
- 840 Maignan, F., Abadie, C., Remaud, M., Kooijmans, L. M. J., Kohonen, K.-M., Commane, R., Wehr, R., Campbell, J. E., Belviso, S., Montzka, S. A., Raoult, N., Seibt, U., Shiga, Y. P., Vuichard, N., Whelan, M. E., and Peylin, P.: Carbonyl sulfide: comparing a mechanistic representation of the vegetation uptake in a land surface model and the leaf relative uptake approach, *Biogeosciences*, 18, 2917–2955, <https://doi.org/10.5194/bg-18-2917-2021>, 2021.
- 845 Masaki, Y., Iizuka, R., Kato, H., Kojima, Y., Ogawa, T., Yoshida, M., Matsushita, Y., and Katayama, Y.: Fungal Carbonyl Sulfide Hydrolase of *Trichoderma harzianum* Strain THIF08 and Its Relationship with Clade D β -Carbonic Anhydrases, *Microbes and Environments*, 36, ME20058, <https://doi.org/10.1264/jsme2.ME20058>, 2021.
- Maseyk, K., Berry, J. A., Billesbach, D., Campbell, J. E., Torn, M. S., Zahniser, M., and Seibt, U.: Sources and sinks of carbonyl sulfide in an agricultural field in the Southern Great Plains, *PNAS*, 111, 9064–9069, 850 <https://doi.org/10.1073/pnas.1319132111>, 2014.
- McNorton, J., Wilson, C., Gloor, M., Parker, R. J., Boesch, H., Feng, W., Hossaini, R., and Chipperfield, M. P.: Attribution of recent increases in atmospheric methane through 3-D inverse modelling, *Atmospheric Chemistry and Physics*, 18, 18149–18168, <https://doi.org/10.5194/acp-18-18149-2018>, 2018.
- Monks, S. A., Arnold, S. R., Hollaway, M. J., Pope, R. J., Wilson, C., Feng, W., Emmerson, K. M., Kerridge, B. J., Latter, B. 855 L., Miles, G. M., Siddans, R., and Chipperfield, M. P.: The TOMCAT global chemical transport model v1.6: description of chemical mechanism and model evaluation, *Geosci. Model Dev.*, 10, 3025–3057, <https://doi.org/10.5194/gmd-10-3025-2017>, 2017.
- Montzka, S. A., Calvert, P., Hall, B. D., Elkins, J. W., Conway, T. J., Tans, P. P., and Sweeney, C.: On the global distribution, seasonality, and budget of atmospheric carbonyl sulfide (COS) and some similarities to CO₂, *J. Geophys. Res.*, 112, 860 <https://doi.org/10.1029/2006JD007665>, 2007.
- Ogée, J., Sauze, J., Kesselmeier, J., Genty, B., Van Diest, H., Launois, T., and Wingate, L.: A new mechanistic framework to predict OCS fluxes from soils, *Biogeosciences*, 13, 2221–2240, <https://doi.org/10.5194/bg-13-2221-2016>, 2016.
- Parker, R. J., Boesch, H., McNorton, J., Comyn-Platt, E., Gloor, M., Wilson, C., Chipperfield, M. P., Hayman, G. D., and Bloom, A. A.: Evaluating year-to-year anomalies in tropical wetland methane emissions using satellite CH₄ observations, 865 *Remote Sensing of Environment*, 211, 261–275, <https://doi.org/10.1016/j.rse.2018.02.011>, 2018.
- Protoschill-Krebs, G., Wilhelm, C., and Kesselmeier, J.: Consumption of carbonyl sulphide (COS) by higher plant carbonic anhydrase (CA), *Atmospheric Environment*, 30, 3151–3156, [https://doi.org/10.1016/1352-2310\(96\)00026-X](https://doi.org/10.1016/1352-2310(96)00026-X), 1996.
- Remaud, M., Chevallier, F., Maignan, F., Belviso, S., Berchet, A., Parouffe, A., Abadie, C., Bacour, C., Lennartz, S., and Peylin, P.: Plant gross primary production, plant respiration and carbonyl sulfide emissions over the globe inferred by 870 atmospheric inverse modelling, *Atmos. Chem. Phys.*, 22, 2525–2552, <https://doi.org/10.5194/acp-22-2525-2022>, 2022.

- Remaud, M., Ma, J., Krol, M., Abadie, C., Cartwright, M. P., Patra, P., Niwa, Y., Rodenbeck, C., Belviso, S., Kooijmans, L., Lennartz, S., Maignan, F., Chevallier, F., Chipperfield, M. P., Pope, R. J., Harrison, J. J., Vimont, I., Wilson, C., and Peylin, P.: Intercomparison of Atmospheric Carbonyl Sulfide (TransCom-COS; Part One): Evaluating the Impact of Transport and Emissions on Tropospheric Variability Using Ground-Based and Aircraft Data, *Journal of Geophysical Research: Atmospheres*, 128, e2022JD037817, <https://doi.org/10.1029/2022JD037817>, 2023.
- 875 Sandoval-Soto, L., Stanimirov, M., von Hobe, M., Schmitt, V., Valdes, J., Wild, A., and Kesselmeier, J.: Global uptake of carbonyl sulfide (COS) by terrestrial vegetation: Estimates corrected by deposition velocities normalized to the uptake of carbon dioxide (CO₂), *Biogeosciences*, 2, 125–132, <https://doi.org/10.5194/bg-2-125-2005>, 2005.
- Seibt, U., Wingate, L., Lloyd, J., and Berry, J. A.: Diurnally variable $\delta^{18}\text{O}$ signatures of soil CO₂ fluxes indicate carbonic anhydrase activity in a forest soil, *Journal of Geophysical Research: Biogeosciences*, 111, <https://doi.org/10.1029/2006JG000177>, 2006.
- 880 Seibt, U., Kesselmeier, J., Sandoval-Soto, L., Kuhn, U., and Berry, J. A.: A kinetic analysis of leaf uptake of COS and its relation to transpiration, photosynthesis and carbon isotope fractionation, *Biogeosciences*, 7, 333–341, <https://doi.org/10.5194/bg-7-333-2010>, 2010.
- 885 Sellers, P. J., Meeson, B. W., Hall, F. G., Asrar, G., Murphy, R. E., Schiffer, R. A., Bretherton, F. P., Dickinson, R. E., Ellingson, R. G., Field, C. B., Huemmrich, K. F., Justice, C. O., Melack, J. M., Roulet, N. T., Schimel, D. S., and Try, P. D.: Remote sensing of the land surface for studies of global change: Models — algorithms — experiments, *Remote Sensing of Environment*, 51, 3–26, [https://doi.org/10.1016/0034-4257\(94\)00061-Q](https://doi.org/10.1016/0034-4257(94)00061-Q), 1995.
- Slevin, D., Tett, S., and Williams, M.: Global GPP simulated by the JULES land surface model for 2001–2010, <https://doi.org/10.7488/ds/1461>, 2016.
- 890 Smith, K. S. and Ferry, J. G.: Prokaryotic carbonic anhydrases, *FEMS Microbiology Reviews*, 24, 335–366, <https://doi.org/10.1111/j.1574-6976.2000.tb00546.x>, 2000.
- Smith, K. S., Jakubzick, C., Whittam, T. S., and Ferry, J. G.: Carbonic anhydrase is an ancient enzyme widespread in prokaryotes, *Proceedings of the National Academy of Sciences*, 96, 15184–15189, <https://doi.org/10.1073/pnas.96.26.15184>, 895 1999.
- Spielmann, F. M., Wohlfahrt, G., Hammerle, A., Kitz, F., Migliavacca, M., Alberti, G., Ibrom, A., El-Madany, T. S., Gerdel, K., Moreno, G., Kolle, O., Karl, T., Peressotti, A., and Delle Vedove, G.: Gross Primary Productivity of Four European Ecosystems Constrained by Joint CO₂ and COS Flux Measurements, *Geophysical Research Letters*, 46, 5284–5293, <https://doi.org/10.1029/2019GL082006>, 2019.
- 900 Spivakovsky, C. M., Logan, J. A., Montzka, S. A., Balkanski, Y. J., Foreman-Fowler, M., Jones, D. B. A., Horowitz, L. W., Fusco, A. C., Brenninkmeijer, C. a. M., Prather, M. J., Wofsy, S. C., and McElroy, M. B.: Three-dimensional climatological distribution of tropospheric OH: Update and evaluation, *Journal of Geophysical Research: Atmospheres*, 105, 8931–8980, <https://doi.org/10.1029/1999JD901006>, 2000.

- Stimler, K., Montzka, S. A., Berry, J. A., Rudich, Y., and Yakir, D.: Relationships between carbonyl sulfide (COS) and CO₂ during leaf gas exchange, *New Phytologist*, 186, 869–878, <https://doi.org/10.1111/j.1469-8137.2010.03218.x>, 2010.
- Stimler, K., Berry, J. A., and Yakir, D.: Effects of Carbonyl Sulfide and Carbonic Anhydrase on Stomatal Conductance, *PLANT PHYSIOLOGY*, 158, 524–530, <https://doi.org/10.1104/pp.111.185926>, 2012.
- Stinecipher, J. R., Cameron-Smith, P. J., Blake, N. J., Kuai, L., Lejeune, B., Mahieu, E., Simpson, I. J., and Campbell, J. E.: Biomass Burning Unlikely to Account for Missing Source of Carbonyl Sulfide, *Geophysical Research Letters*, 46, 14912–14920, <https://doi.org/10.1029/2019GL085567>, 2019.
- Sun, W., Kooijmans, L. M. J., Maseyk, K., Chen, H., Mammarella, I., Vesala, T., Levula, J., Keskinen, H., and Seibt, U.: Soil fluxes of carbonyl sulfide (COS), carbon monoxide, and carbon dioxide in a boreal forest in southern Finland, *Atmospheric Chemistry and Physics*, 18, 1363–1378, <https://doi.org/10.5194/acp-18-1363-2018>, 2018.
- Suntharalingam, P., Kettle, A. J., Montzka, S. M., and Jacob, D. J.: Global 3-D model analysis of the seasonal cycle of atmospheric carbonyl sulfide: Implications for terrestrial vegetation uptake, *Geophys. Res. Lett.*, 35, 6, <https://doi.org/10.1029/2008GL034332>, 2008.
- Watts, S. F.: The mass budgets of carbonyl sulfide, dimethyl sulfide, carbon disulfide and hydrogen sulfide, *Atmospheric Environment*, 34, 19, 2000.
- Whelan, M. E., Min, D.-H., and Rhew, R. C.: Salt marsh vegetation as a carbonyl sulfide (COS) source to the atmosphere, *Atmospheric Environment*, 73, 131–137, <https://doi.org/10.1016/j.atmosenv.2013.02.048>, 2013.
- Whelan, M. E., Lennartz, S. T., Gimeno, T. E., Wehr, R., Wohlfahrt, G., Wang, Y., Kooijmans, L. M. J., Hilton, T. W., Belviso, S., Peylin, P., Commane, R., Sun, W., Chen, H., Kuai, L., Mammarella, I., Maseyk, K., Berkelhammer, M., Li, K.-F., Yakir, D., Zumkehr, A., Katayama, Y., Ogée, J., Spielmann, F. M., Kitz, F., Rastogi, B., Kesselmeier, J., Marshall, J., Erkkilä, K.-M., Wingate, L., Meredith, L. K., He, W., Bunk, R., Launois, T., Vesala, T., Schmidt, J. A., Fichot, C. G., Seibt, U., Saleska, S., Saltzman, E. S., Montzka, S. A., Berry, J. A., and Campbell, J. E.: Reviews and syntheses: Carbonyl sulfide as a multi-scale tracer for carbon and water cycles, *Biogeosciences*, 15, 3625–3657, <https://doi.org/10.5194/bg-15-3625-2018>, 2018.
- Whelan, M. E., Shi, M., Sun, W., Vries, L. K., Seibt, U., and Maseyk, K.: Soil Carbonyl Sulfide (OCS) Fluxes in Terrestrial Ecosystems: An Empirical Model, *Journal of Geophysical Research: Biogeosciences*, 127, e2022JG006858, <https://doi.org/10.1029/2022JG006858>, 2022.
- Wilson, C., Gloor, M., Gatti, L. V., Miller, J. B., Monks, S. A., McNorton, J., Bloom, A. A., Basso, L. S., and Chipperfield, M. P.: Contribution of regional sources to atmospheric methane over the Amazon Basin in 2010 and 2011, *Global Biogeochemical Cycles*, 30, 400–420, <https://doi.org/10.1002/2015GB005300>, 2016.
- Zumkehr, A., Hilton, T. W., Whelan, M., Smith, S., Kuai, L., Worden, J., and Campbell, J. E.: Global gridded anthropogenic emissions inventory of carbonyl sulfide, *Atmospheric Environment*, 183, 11–19, <https://doi.org/10.1016/j.atmosenv.2018.03.063>, 2018.